# In situ flux estimates reveal large variations in methane flux across the bottom boundary layer of a eutrophic lake

**Sofia L. D'Ambrosio** [ORCID],* **Stephen M. Henderson** [ORCID], **Jeffrey R. Nielson, John A. Harrison** [ORCID]
Washington State University Vancouver, School of the Environment, Vancouver, Washington

## Abstract

Methane ($CH_4$) produced in anoxic sediments plays a significant role in the carbon economy of many lakes and reservoirs. $CH_4$ released from sediments first crosses the bottom boundary layer (BBL), the layer of water overlying the lakebed where currents are slowed by friction with the sediments below. Physical and biogeochemical conditions in the BBL, which can fluctuate hourly to daily with basin-wide internal waves (seiches), likely influence $CH_4$ transport from sediments into the hypolimnion. In this study, we estimated $CH_4$ fluxes across the BBL of a eutrophic lake using a novel in situ flux gradient approach adapted from marine applications. For 2–6 h periods throughout the spring and summer, we estimated $CH_4$ fluxes across the BBL using simultaneous measurements of $CH_4$ concentrations, turbulent mixing, and thermal stratification. Sub-daily variation in $CH_4$ fluxes was high, and $CH_4$ fluxes sometimes changed several-fold within hours. These rapid shifts in BBL fluxes were likely influenced by fluctuations in seiche-driven variations in the intensity of BBL turbulent mixing. Fluxes increased from spring to summer, concurrent with the development of lake stratification, and fueled an accumulation of $CH_4$ below the thermocline. Throughout the summer, $CH_4$ flux across the BBL exceeded $CH_4$ accumulation below the thermocline, suggesting significant methanotrophy in the hypolimnion, consistent with incubation-based oxidation rates. Our results are the first to demonstrate sub-daily and seasonal variability in the timing and magnitude of $CH_4$ fluxes within a lake BBL, and highlight a need to quantify such variability in other lentic systems.

Lakes and reservoirs are globally significant sources of methane ($CH_4$), contributing an estimated 70–175 Tg of $CH_4$ to the atmosphere per year (Rosentreter et al. 2021). Methanogenesis in anoxic sediments is a primary source of $CH_4$ in most lakes and reservoirs (Bastviken 2009), although the significance of oxic $CH_4$ production in the water column is an ongoing area of research (Günthel et al. 2019; Peeters and Hofmann 2021). Quantifying the flux and fate of $CH_4$ released from lake sediments is particularly important during summertime thermal stratification in monomictic and dimictic lakes. The development of stratification slows vertical mixing between the epilimnion and hypolimnion. Methane diffusing from sediments during this stratified period can either accumulate in the hypolimnion, undergo bacterial oxidation, or slowly diffuse across the thermocline into the epilimnion. A significant portion of $CH_4$ accumulated in the hypolimnion during a stratified period can eventually be emitted during lake turnover (Kankaala et al. 2007; Encinas Fernández et al. 2014). Therefore, characterizing the magnitude, variability, and fate of $CH_4$ flux from lake sediments into the hypolimnion is crucial for understanding lentic greenhouse gas dynamics and emissions to the atmosphere.

A critical interface between the primary site of $CH_4$ production (sediments) and $CH_4$ storage (the hypolimnion) is the bottom boundary layer (BBL; Fig. 1), a region extending up to several meters above the lake sediment where currents are strongly affected by bottom friction (Wüest and Lorke 2003). The BBL can be further divided into multiple sublayers (Fig. 1), each governed by different physical controls (Henderson and Nielson 2021). Here, we focus on $CH_4$ flux through the turbulent BBL, which extends from several centimeters to potentially several meters above the sediment. Chemical transport in this layer is dominated by turbulent diffusion, which mixes water and solutes much more rapidly than molecular diffusion.

The large seasonal and daily variability in conditions within the turbulent BBL likely has important, but unexplored,

Additional Supporting Information may be found in the online version of this article.

implications for CH$_4$ flux and fate in the hypolimnion of stratified lakes. On a seasonal basis, thermal stratification can lead to the depletion of oxygen, nitrate, and other terminal electron acceptors in the BBL and hypolimnion (Eckert and Conrad 2007; Deemer and Harrison 2019). The resulting anoxia facilitates CH$_4$ flux into the hypolimnion (Hounshell et al. 2021), and seasonal shifts in CH$_4$ and electron acceptor concentrations may stimulate rapid responses in methanotrophy in the water column (Saarela et al. 2020; Mayr et al. 2020*a*, *b*). On an hourly to daily basis, many lakes experience a basin-wide internal wave (or seiche) that drives fluctuations in BBL conditions (Wüest and Lorke 2003). The seiche cycle can trigger periods of intense turbulent mixing in the BBL, which are sometimes followed by relatively quiescent periods where thermal stratification can significantly inhibit turbulent mixing (Henderson 2016*a*). Broadly, fluctuations in turbulent mixing rates above the sediment are known to cause fluctuations in diffusive boundary layer thickness, affecting sediment–water fluxes of oxygen and other compounds (Lorke et al. 2003; Brand et al. 2009). In some lakes, such fluctuations in turbulent mixing rates are specifically tied to the seiche cycle, generating intense variability in fluxes of oxygen (Brand et al. 2008; Bryant et al. 2010) and in gradients of nitrogenous compounds (Deemer et al. 2015) in the turbulent BBL.

Despite the potential for BBL conditions to influence CH$_4$ dynamics in the hypolimnion, common methods for quantifying the flux and fate of sediment-derived CH$_4$ in stratified lakes largely ignore variability in BBL conditions. For example, CH$_4$ flux from sediments is often measured using benthic chambers (Kuivila et al. 1988), porewater profiles (Huttunen et al. 2006), or ex situ incubations (Liikanen et al. 2002), none of which can account for variable BBL mixing. Mass balance approaches to determine the fate of sediment-derived CH$_4$ frequently rely on daily-averaged to seasonally-averaged CH$_4$ concentration profiles and estimates made well above the BBL (Bastviken et al. 2008), thus ignoring any short-term variability in lake mixing or biogeochemistry. Furthermore, some methods that are useful for resolving short-term variability in solute fluxes that can be measured rapidly, such as eddy correlation, cannot be used to estimate fluxes of CH$_4$ or other solutes for which fast-response sensors are unavailable. Owing to these methodological challenges, previous studies of the interplay between lake BBL conditions and CH$_4$ dynamics have been limited to a single study modeling sediment CH$_4$ oxidation (Brand et al. 2009). In that study, seiche-driven changes in the diffusive BBL (Fig. 1) had little effect on rates of methanotrophy within the uppermost layers of sediment. However, no studies to-date have investigated how CH$_4$ transport above the sediment, within the turbulent BBL, is influenced by seiche-induced dynamic forcing.

In this paper, we overcome these limitations by modifying and applying a flux gradient approach. This approach estimates fluxes as a function of vertical gradients in chemical concentrations, which can be measured in the BBL using
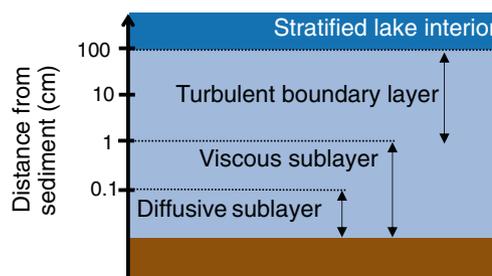


**Fig. 1.** Schematic showing layers of the BBL, as often observed in the hypolimnion immediately above a lakebed (note log scale on vertical axis).

recent advances in sampling and instrumentation (Sauter et al. 2005; Holtappels et al. 2011; Knoery et al. 2019). Within the BBL, the flux gradient technique has been used to estimate fluxes of oxygen, total alkalinity, and momentum in marine systems (Reidenbach et al. 2006; McGillis et al. 2011; Turk et al. 2015; Takeshita et al. 2016). However, these BBL studies assumed an unstratified turbulent BBL, within which logarithmic boundary layer theory can be applied. This assumption is often violated in strongly stratified low-energy flows (Holtappels and Lorke 2011), which are common in small lakes and reservoirs (Henderson 2016*a*). An alternative assumption of constant mixing efficiency, applicable to stratified low-energy conditions, has been used to obtain flux gradient estimates of nitrate fluxes across the thermocline in the ocean (Sharples et al. 2007; Williams et al. 2013). However, this approach becomes inapplicable in weakly stratified, high-energy flows, which can also occur in lake BBLs. Here, using generalized mixing parameterizations developed by previous researchers, we adapt the flux gradient approach for application across a range of cases, from high-energy logarithmic boundary layer cases to low-energy stratified conditions. We apply the flux gradient method for the first time to the lake BBL environment, yielding the first non-invasive estimates of BBL CH$_4$ fluxes.

We estimate CH$_4$ fluxes across the BBL of a eutrophic, monomictic reservoir before and during summer stratification. We combine fluxes estimated over multiple 2–6 h periods with simultaneous monitoring of turbulent mixing, stratification, temperature, and dissolved oxygen (DO) concentrations within the BBL. Our goal was to characterize the magnitude and variability of CH$_4$ fluxes within the BBL across short-term (sub-daily) and longer (seasonal) time scales and determine the fate of BBL CH$_4$ in the lake hypolimnion. In addition, we compare our results from the flux gradient approach with flux estimates obtained previously in other lakes using conventional methods.

## Methods

### Study system

Lacamas Lake is a eutrophic, monomictic reservoir located in southwestern Washington State, USA (Fig. 2). The reservoir has a
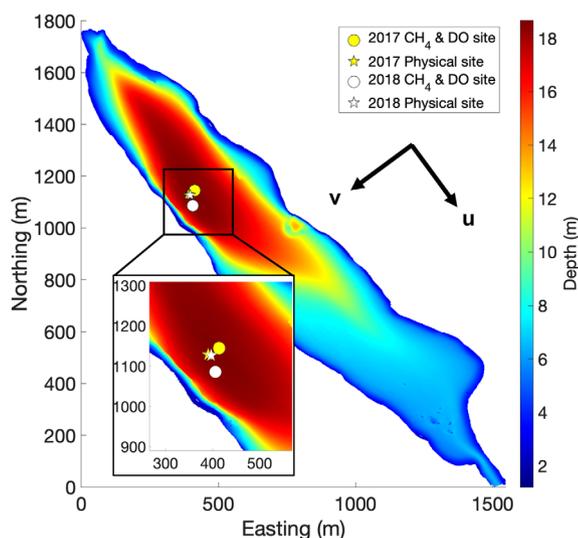
**Fig. 2.** Bathymetric map of Lacamas Lake with close-up of sampling sites (inset). Circles indicate sites for CH₄ and DO sampling. Stars indicate locations for physical (temperature and velocity) sampling. Locations for 2017 are shown in yellow and 2018 in white. Arrows indicate direction of along-lake velocity ($u$) and across-lake velocity ($v$), and the length of arrows are not quantitatively to scale. Origin of bathymetric map is 45.6098°N, 122.4366 W°.

surface area of 1.3 km$^2$, an average depth of 7.8 m, and a maximum depth of 18 m. Rates of surface CH₄ emission from Lacamas are comparable to rates from other eutrophic reservoirs, averaging 66 mg CH₄ m$^{-2}$ d$^{-1}$ (Deemer et al. 2016; Harrison et al. 2017). During summer, a metalimnion develops between 4 and 7 m depth, which largely inhibits mixing between the epilimnion and hypolimnion (Deemer et al. 2011). After the onset of stratification, CH₄ accumulates below the metalimnion (Deemer and Harrison 2019).

Our study focuses on conditions in the bottom meter of the BBL in Lacamas, where velocity, turbulent mixing, and temperature are strongly influenced by a wind-driven, basin-wide seiche (Henderson and Deemer 2012; Deemer et al. 2015; Henderson 2016a,b). Temporal seiche-induced temperature fluctuations are small compared to top-to-bottom temperature fluctuations during mid- and late-summer, indicating that strong stratification prevents overturning (Henderson and Deemer 2012). Correspondingly, previous work (Nielson and Henderson 2022) determined the seiche in Lacamas to be in the damped, linear regime during the summer (Horn et al. 2001). The seiche is responsible for velocity fluctuations with a period of approximately 10–24 h (Henderson and Deemer 2012; Henderson 2016a). Owing to the lake's narrow geometry, along-lake velocities ($u$) are generally larger than across-lake velocities ($v$, Fig. 2). In Lacamas, the energy flux carried by net vertical seiche propagation approximately balances the production of turbulent kinetic energy in the BBL (Henderson 2016a). Bursts of high-energy turbulent mixing in the BBL of the deep-water region follow bursts of strong wind

forcing by 1–2 d, as expected given the time for vertical propagation of energy by the seiche (Henderson 2016a).

### Water column characterization

Profiles of temperature, DO, and CH₄ spanning the full water column were used to characterize the development of thermal and chemical stratification in Lacamas and to quantify CH₄ storage in the hypolimnion. Water column sampling was performed at the deepest part of the lake (18 m depth, Fig. 2) approximately bimonthly between April and September of 2017 and 2018. A Hydrolab DS5X Sonde measured temperature and DO every 1–3 m throughout the water column. CH₄ concentrations were determined via headspace equilibration at the same depths using duplicate water samples collected with a Van Dorn sampler. This process consisted of flushing and filling glass serum vials (70 mL) with water from each depth, fixing samples with saturated ZnCl₂, and crimp sealing filled vials using gray butyl septa. Less than 10% of samples contained bubbles and they were discarded. Vials were injected with a 20 mL pure helium headspace, shaken thoroughly, and allowed to equilibrate for at least 24 h. Headspace CH₄ concentrations were then measured on an HP 5890 gas chromatograph with a flame ionization detector (Deemer and Harrison 2019) with a precision of ± 5% over the range of CH₄ concentrations analyzed. Aqueous concentrations were calculated using Bunsen temperature-specific solubility coefficients (Wanninkhof 1992).

### BBL sampling locations

To estimate CH₄ fluxes in the BBL, profiles of CH₄, DO, velocity, and temperature were characterized in the bottom meter of Lacamas near the lake's deepest point (Fig. 2) from May to August 2017 and in May 2018. In both years, chemical (CH₄ and DO) and physical (temperature and velocity) profiles were measured simultaneously. To minimize flow disturbances for velocity measurements, physical sampling sites were separated from chemical sampling sites by 28 and 42 m in 2017 and 2018, respectively (Fig. 2). To evaluate if physical mixing conditions at the two sites were similar, temperatures were monitored at the same three elevations ($z = 0.1$, 0.4, and 0.9 m above the lakebed) at the chemical sampling site and the physical sampling site. Both sets of temperatures were found to be in excellent agreement (for 2017, linear regression yields $T_{chem} = 0.99 \, (T_{phys}) + 0.04°C$ with $R^2 = 0.99$; for 2018, $T_{chem} = 1.00 \, (T_{phys}) + 0.02°C$ with $R^2 = 0.99$).

### BBL methane and oxygen sampling

BBL methane profiles were measured every 5–10 min for periods of 2–6 h on each CH₄ flux sampling date (approximately bimonthly from April to August 2017 and on four dates in May 2018). Gas-impermeable, opaque Viton fluoroelastomer tubing (1/8″ ID, McMaster-Carr) was fastened to a 1.5-m tall aluminum tripod resting on the lakebed. Separate lines of tubing were used to draw water samples at elevations of $z = 0.1$ and $z = 0.9$ m above the lakebed in 2017; in 2018, a third line of tubing was

added at $z = 0.4$ m. DO was measured every minute using PME miniDOT loggers mounted at the same elevations as $CH_4$ sampling tubes. Tubing and oxygen loggers were arranged to minimize flow disturbance.

To measure $CH_4$ profiles in the BBL on each $CH_4$ flux sampling date, paired water samples from each elevation were slowly and simultaneously pulled up from depth every 5–10 min using 60-mL BD luer lok syringes connected to the tubing. The entire tubing volume was flushed once before each sampling pull. Water samples from the BBL were then processed for $CH_4$ concentrations as described above for the water column $CH_4$ profiles, but with smaller glass serum vials (27 mL water volume with a 10 mL helium headspace).

### BBL velocity and temperature sampling

Profiles of water velocity and temperature within the BBL were used to determine rates of physical mixing, as required for $CH_4$ flux calculations. Variables involved in physical mixing rate and flux calculations are summarized in Supporting Information Table S1. Velocity and temperature were measured from April to September in 2017 and from April to May in 2018. Temperature profiles were measured by a vertical array of RBR Solo T thermistors (error $\pm$ 0.01°C), attached to an aluminum frame with a vertical line and held taut by a subsurface buoy. These instruments recorded temperature every 4 s at nine elevations (approximately every 0.1 m) from 0.18 to 0.86 m (2017) or 0.17 to 0.93 m (2018) above the lakebed, and half-hourly averages are presented.

Profiles of velocity were measured using two adjacent, upward-facing 2-MHz Nortek Aquadopp Acoustic Doppler Current Profilers (ADCPs) mounted together on an aluminum frame resting on the lakebed, with acoustic transducers about 0.04 m above the bed. Each ADCP operated in pulse-coherent mode and recorded velocity profiles during one 0.5-s interval every 15 s. Velocity profiles were recorded between 0.15 and 0.90 m above the bed, with 0.015 m vertical resolution. The two ADCPs yielded two time series of half-hourly averaged horizontal velocity. These two time series were in excellent agreement and were averaged for all results presented here.

### N² estimation

The squared buoyancy frequency $N^2$, an indicator of the strength of stratification used in the estimation of $CH_4$ fluxes, was estimated between each instrument pair in the temperature profile:

$$N^2 = \frac{-g}{\rho_0} \frac{\partial \rho}{\partial z}, \qquad (1)$$

where $g$ is gravitational acceleration (9.81 m s$^{-2}$), $\rho$ is the density at elevation $z$ above the lakebed (kg m$^{-3}$) as a function of temperature, and $\rho_0$ is the mean density of the temperature profile (Thorpe 2007). Estimated $N^2$ error was approximately $\pm 1 \times 10^{-4}$ s$^{-2}$, based on RBR thermistor errors ($\pm$ 0.01°C).

### Turbulent dissipation rate estimation

The rate of viscous dissipation of turbulent energy ($\mathcal{E}$), an indicator of the strength of turbulent mixing used in the estimation of methane fluxes, was estimated along vertical profiles using a structure–function method based on Wiles et al. (2006). First, spatial velocity variability is quantified by:

$$\beta(z,r) = w\left(\tilde{z} + r/2\right) - w\left(\tilde{z} - r/2\right), \qquad (2)$$

where $w(\zeta)$ is the velocity measured a distance $\zeta$ along one of the ADCP acoustic beams, $\tilde{z} = z/\cos(25°)$ is the along-beam distance corresponding to elevation $z$, and the factor $\cos(25°)$ accounts for beam tilt (Wiles et al. 2006). One $\beta$ time series was calculated for every pair of rangebins along an acoustic beam, so that along-beam separation $r$ equaled 1, 2, 3, or 4 bins. To separate turbulence from long period motions such as currents and internal waves, a 4-min running mean was subtracted from each $\beta$ time series, with deviations from the running mean denoted by $\beta'$. The magnitude of small-scale turbulent velocity fluctuations was then quantified by the variance of $\beta'(z,r)$, that is:

$$Q(z,r) = \overline{\beta'^2(z,r)}, \qquad (3)$$

where the overbar denotes averaging over a half-hour interval. For each $r$, further statistical stability was obtained by averaging over all $Q(z,r)$ values in 10-cm vertical $z$ bins.

The differencing used to calculate $\beta$ removes motions with scales much larger than $r$. Therefore $Q(z,r)$ approaches zero as $r$ approaches zero. Specifically, the theory of homogeneous inertial subrange turbulence suggests:

$$Q(z,r) = C(\mathcal{E}r)^{2/3}, \qquad (4)$$

where the empirical constant $C \approx 2$ (Monin and Yaglom 1975). Therefore, at each height, the dissipation rate $\mathcal{E}(z)$ is estimated as $A^{3/2}$, where $A$ is the slope of a linear regression between $Q(z,r)$ and $r^{2/3}$. Since stratification invalidates the underlying inertial-subrange theory at large (Ozmidov) scales, separations of more than four rangebins are excluded from the regression. At each elevation $z$, one $\mathcal{E}$ estimate is obtained from each of the six acoustic beams of the two ADCPs, and the median of these six estimates is reported.

Turbulent dissipation rate measurements were used for estimating the thickness of the diffusive and viscous sublayers in the BBL (Fig. 1). These sublayer thicknesses were not directly used to calculate $CH_4$ fluxes, but they are useful as indicators of transport across the sediment–water interface. Specifically, relatively high sublayer thickness indicates high resistance to flux across the sediment–water

interface, whereas lower thickness is associated with more rapid diffusion. Following Lorke et al. (2003), the thickness of the viscous sublayer ($\delta_\nu$) was calculated as:

$$\delta_\nu = \frac{11\nu}{(\kappa z_1 \varepsilon_1)^{1/3}}, \tag{5}$$

where $\nu$ is the kinematic viscosity of water (m$^2$ s$^{-1}$), $\kappa$ is the dimensionless constant 0.4, $z_1$ is the elevation of the lowest $\mathcal{E}$ estimate (m), and $\varepsilon_1$ is the corresponding turbulent dissipation rate at $z_1$ (W/kg). Diffusive sublayer thickness ($\delta_d$) was calculated as:

$$\delta_d = S_c^{-\alpha} \delta_\nu, \tag{6}$$

where $S_c$ is the Schmidt number and $\alpha$ is the dimensionless constant 0.33 (Lorke and MacIntyre 2009). We assume $S_c$ as $1.31 \times 10^3$, as appropriate for the kinematic viscosity of water and molecular diffusivity of solutes within the temperature range of the BBL in Lacamas (about $1.31 \times 10^{-6}$ and $10^{-9}$ m$^2$ s$^{-1}$, respectively, at 10°C.)

**Methane flux estimation**

Methane fluxes at an elevation $z$ in the turbulent BBL were estimated by adapting a flux gradient approach previously used in marine applications:

$$F_{BBL} = -D \frac{\partial C}{\partial z}, \tag{7}$$

where $F_{BBL}$ is the CH$_4$ flux, $D$ is the turbulent diffusivity, and $\frac{\partial C}{\partial z}$ is the derivative of CH$_4$ concentration with depth. Similar expressions are often used to estimate chemical fluxes across the diffusive sublayer. However, the turbulent diffusivity in Eq. 7 represents mixing at elevations well above the diffusive sublayer, and greatly exceeds the molecular diffusivity. Correspondingly, the gradient $\partial C/\partial z$ is weaker in the turbulent BBL than within the diffusive sublayer. Rearranging Eq. 7, assuming a constant flux between sampling elevations $z_1$ and $z_2$, and integrating with respect to depth gives:

$$F_{BBL} = -k_{BBL}(C_{z_2} - C_{z_1}), \tag{8}$$

where $(C_{z_2} - C_{z_1})$ indicates the average CH$_4$ concentration gradient (mmol m$^{-3}$) between sampling elevations $z_1$ and $z_2$ and the corresponding piston velocity (m s$^{-1}$) is $k_{BBL} = \left( \int_{z_1}^{z_2} \frac{dz}{D} \right)^{-1}$ (Fig. 3). In 2017, $z_1$ and $z_2$ were, respectively, 0.1 and 0.9 m above the bed. In 2018, two pairs of $z_1$ and $z_2$ were used: 0.1 and 0.4 m (hereafter the inner BBL) or 0.4 and 0.9 m (hereafter the outer BBL). Methane fluxes from Eq. 8 were calculated on a half-hourly basis, and then pooled together into hourly averages to increase statistical power.

Diffusivity $D$, used in the estimation of $k_{BBL}$, was calculated using a modified Osborn method (Osborn 1980):

$$D = \frac{\Gamma \mathcal{E}}{N^2}, \tag{9}$$

where $\Gamma$ is the mixing efficiency coefficient. We estimated $\frac{\Gamma}{N^2}$ as:

$$\frac{\Gamma}{N^2} = \left[ 0.7\, e^{(-5.7\, \mathrm{Ri_g})} S^2 + 4N^2 \right]^{-1}, \tag{10}$$

where $S^2$ is shear $\left( [\partial \overline{u}/\partial z]^2 + [\partial \overline{v}/\partial z]^2 \right)$ of half-hourly mean along-lake ($\overline{u}$) and across-lake ($\overline{v}$) velocities and $\mathrm{Ri_g}$ is the gradient Richardson number $\left( \frac{N^2}{S^2} \right)$. Equation 10 closely resembles Eq. 6 of Nielson and Henderson (2022), written in a form that remains finite in the unstratified ($N^2 \to 0$) limit. As explained by Nielson and Henderson (2022), Eq. 10 is derived from a parameterization by Venayagamoorthy and Stretch (2010). The output of Eq. 10 is multiplied by $\mathcal{E}$ to calculate diffusivity $D$ (Eq. 9), which in turn is used to determine $k_{BBL}$ for estimating CH$_4$ flux (Eq. 8).

Equations 9–10 recover the formulas used in previous marine applications of the flux gradient technique in appropriate limits. In the limit of a weakly stratified logarithmic boundary layer, $D = \kappa u_* z / \mathrm{Pr_T}$ is recovered, where $\mathrm{Pr_T} = 0.7$ is the turbulent Prandtl number for unstratified flow (this is established by setting $\mathrm{Ri_g}$ and $N^2$ to zero on the right of Eq. 10, substituting Eq. 10 into Eq. 9, and using the standard results $S = u_*/(\kappa z)$ and $\varepsilon = u_*^3/(\kappa z)$ from the theory of logarithmic boundary layers). This expression was assumed in previous applications of the flux gradient technique to marine BBLs (McGillis et al. 2011; Takeshita et al. 2016), although these authors adopted the simplification $\mathrm{Pr_T} = 1$. In the limit of strongly stratified (high $\mathrm{Ri_g}$) flow, $\Gamma = 0.25$ is recovered, which closely resembles previous applications of the flux gradient technique to regions above the BBL (Sharples et al. 2001, 2007; Williams et al. 2013). The transition from weakly to strongly stratified conditions, and the associated transition in $\Gamma$ values, is an ongoing area of research (Venayagamoorthy and Stretch 2010; Gregg et al. 2018; Monismith et al. 2018). However, our conclusions were not sensitive to the details of $\Gamma$ parameterization. Applying an alternative parameterization for $\Gamma$ (Monismith et al. 2018) resulted in flux estimates similar to those calculated using the approach described above.

**Adjusting for low Reynolds number conditions**

Our approach to calculating CH$_4$ fluxes in the BBL assumes the turbulent diffusivity for heat ($D$ from Eq. 9) is a suitable proxy for the turbulent diffusivity of CH$_4$. However, solutes may be mixed more slowly than heat in some very low-energy stratified cases (Smyth et al. 2005), that is, in cases with low values of the buoyancy Reynolds number $\mathrm{Re_b} = \frac{\mathcal{E}}{\nu N^2}$. We account for this by approximating the relationship between $\mathrm{Re_b}$ and the turbulent diffusivity of salinity observed by Smyth et al. (2005):
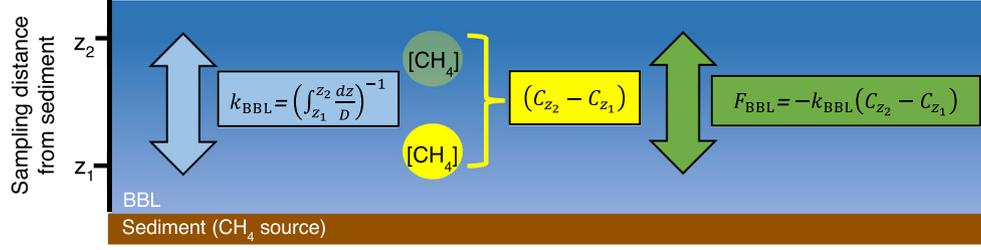
**Fig. 3.** Conceptual diagram of CH$_4$ flux estimates. Estimates of piston velocity $k_{BBL}$ and CH$_4$ flux $F_{BBL}$ are indicated with the blue and green arrows, respectively. Circles indicate CH$_4$ concentrations, with the more opaque yellow circle representing a higher CH$_4$ concentration. Estimates of CH$_4$ gradient $(C_{z_2} - C_{z_1})$ represented by the yellow bracket.

$$D_a = \begin{cases} D, & \mathrm{Re}_b > 100 \\ D\left(\frac{\mathrm{Re}_b}{100}\right)^{1/4}, & \mathrm{Re}_b < 100 \end{cases} \qquad (11)$$

where $D_a$ is the adjusted diffusivity and $D$ is the diffusivity estimated from Eq. 9. This expression was chosen to fit the data in Fig. 15 of Smyth et al. (2005).

Mixing becomes very weak, and poorly understood, when $\mathrm{Re}_b$ is less than about 20 (Stillinger et al. 1983). In such cases, flux estimates presented here may have been subject to large relative errors, even with the diffusivity adjustment in Eq. 11. However, fluxes during such very low-energy cases are small and did not contribute greatly to total estimated CH$_4$ transport (see "Discussion" section).

### Statistical analysis

To analyze monthly differences in CH$_4$ flux in 2017, hourly flux estimates from each sampling date were grouped by month. Each month was individually tested for normality with an Anderson–Darling test and constant variance was assessed across months with Bartlett's test. Differences across months were then assessed using a non-parametric Kruskal–Wallis test and Dunn's post hoc test. To analyze the hourly time series presented from 2018, fluxes were grouped by sampling height (inner or outer BBL fluxes) and by hour. Each flux group was individually tested for normality with an Anderson–Darling test. Depending on whether the normality assumption was met, each group was then analyzed with a one-sample *t*-test or Wilcoxon signed rank test to determine if each hourly flux group was significantly different from zero.

### Hypolimnetic CH$_4$ balance

Methane fluxes measured in the BBL during 2017 were time-averaged to approximate the daily supply of CH$_4$ from the BBL to the hypolimnion during summer stratification. Trapezoidal integration was performed on the CH$_4$ flux time series for sampling date. Integrated values were divided by the total sampling time (usually 2–6 h d$^{-1}$; see "BBL methane and oxygen sampling" section) to calculate one time-averaged flux for each of the two sampling dates per month, and the monthly mean is presented.

The mass storage of CH$_4$ in the hypolimnion, as well as the hypolimnetic accumulation rate of CH$_4$, were calculated for summer 2017 as in Deemer et al. (2011) using water column CH$_4$ concentration profiles. Briefly, Lacamas was divided into an epilimnion (< 4 m depth), a metalimnion (4–7 m depth), and a hypolimnion (> 7 m depth). The hypolimnion was subdivided into layers based on the depths at which CH$_4$ concentrations were measured bimonthly (see "Water column characterization" section). The volume of each layer was determined using bathymetric data from the Washington Department of Ecology (Deemer and Harrison 2019). The mass of CH$_4$ in each layer was then calculated using the layer's volume and CH$_4$ concentration. Methane masses from each layer were summed to determine total hypolimnetic CH$_4$ mass for each sampling date. The accumulation rate in the hypolimnion was then calculated as the change in hypolimnetic CH$_4$ mass between subsequent sampling dates, divided by the days in between dates and the surface area of the hypolimnion. This approach assumes that CH$_4$ is well mixed horizontally. Monthly averages of hypolimnetic CH$_4$ accumulation rates are presented.

Methane flux across the metalimnion $F_{meta}$ (mmol m$^{-2}$ d$^{-1}$) in summer 2017 was calculated using Fick's first law:

$$F_{meta} = K_{meta} \frac{dC}{dz}, \qquad (12)$$

where $K_{meta}$ is eddy diffusivity (m$^2$ d$^{-1}$) and $\frac{dC}{dz}$ is the vertical derivative of CH$_4$ concentration evaluated across the summer metalimnion (4–7 m depth from the surface). $K_{meta}$ was calculated over multiple 3- to 25-d intervals in summer 2017 using the heat budget method (Jassby and Powell 1975). An average monthly $F_{meta}$ was calculated using monthly averages of $K_{meta}$ and water column profiles of CH$_4$ and temperature (see "Water column characterization" section).

### Hypolimnetic oxidation rates

Oxidation rates in the hypolimnion in summer 2017 were determined using a combination of incubations and previous studies in Lacamas. Incubation samples collected on 04 June 2017 and 17 July 2017 were used to determine oxidation rates in June and July 2017, respectively. On each date, 16 glass

serum vials (70 mL) were flushed and filled with water drawn from 0.9 m above the bed using the tubing system described earlier (see "BBL methane and oxygen sampling" section). Half of the vials were fixed immediately with saturated $ZnCl_2$, whereas the other half were wrapped in foil and incubated in the dark in a water bath at in situ temperature (10°C). After 24 h, the incubated vials were terminated with saturated $ZnCl_2$. All vials were analyzed for aqueous $CH_4$ concentrations via headspace equilibration as described earlier (see "Water column characterization" section). Oxidation rates (mmol $L^{-1}$ $d^{-1}$) were calculated as the linear slope of $CH_4$ concentrations vs. time in the vials.

Incubations were not performed in August 2017, therefore August hypolimnetic oxidation rates $R_{ox}$ (mmol $L^{-1}$ $d^{-1}$) were estimated based on the first-order rate law for $CH_4$ oxidation in Lacamas from Reed et al. (2017):

$$R_{ox} = m(C_{hypo}),  \quad (13)$$

where $m$ is the first-order rate constant for $CH_4$ oxidation (0.12 $d^{-1}$) observed previously in incubations of hypolimnetic water in Lacamas (Reed et al. 2017) and $C_{hypo}$ is the mean hypolimnetic concentration of $CH_4$ (mmol $L^{-1}$). $C_{hypo}$ in August 2017 (0.2–0.3 mmol $L^{-1}$) was within the range of $CH_4$ concentrations at which Reed et al. (2017) fit the relationship in Eq. 13. However, Reed et al. (2017) sampled in the fall, when significantly larger concentrations of terminal electron acceptors were present in the anoxic hypolimnion than in summer. Therefore, oxidation rates presented here for August should be considered potentials, and in situ rates in August may have been lower than predicted by Eq. 13 because the supply of terminal electron acceptors was more limited during our sampling. Oxidation rates from incubations or Eq. 13 were converted to per-area units (mmol $m^{-2}$ $d^{-1}$) using the volume and surface area of the Lacamas hypolimnion (Deemer and Harrison 2019).

Potential terminal electron acceptors for $CH_4$ oxidation in the hypolimnion of Lacamas were assessed as in Reed et al. (2017). Briefly, monthly water column profiles of DO, nitrate ($NO_3^-$), and sulfate ($SO_4^{2-}$) were used to approximate the concentration of electron acceptors available for $CH_4$ oxidation in the hypolimnion. The stoichiometric relationships between these electron acceptors and known $CH_4$ oxidation pathways (Reed et al. 2017) were used to determine the potential for DO, $NO_3^-$, or $SO_4^{2-}$ to explain observed $CH_4$ oxidation rates. Manganese and iron concentrations were not measured because they are small contributors to the terminal electron pool in Lacamas (Reed et al. 2017).

## Results
### Overview
The results presented below are divided into sections describing sub-daily, then seasonal trends in BBL mixing, $CH_4$

and DO concentrations, and $CH_4$ fluxes. On sub-daily time-scales, a key finding is that the upward $CH_4$ flux displays intense variability within the BBL. $CH_4$ flux pulses were observed during intervals of intense, seiche-driven turbulent mixing, whereas weaker, near-zero fluxes were often observed during low-energy stratified conditions. On seasonal timescales, $CH_4$ flux within the BBL increased almost two orders of magnitude from spring to summer. This increase coincided with the development of lakewide stratification and the onset of hypoxia then anoxia in the hypolimnion. Although the summertime increase in $CH_4$ flux fueled some hypolimnetic $CH_4$ accumulation, most of the $CH_4$ transported across the BBL was ultimately oxidized in the hypolimnion.

### Sub-daily mixing and stratification
The main driver of mixing in the BBL was a seiche with a period of 10–24 h (Deemer et al. 2015; Henderson 2016*a*, 2016*b*). An example of the oscillating flows of the seiche over a 5-d period in May 2018 is shown in Fig. 4. Seiche-driven velocity fluctuations (Fig. 4a) were associated with sub-daily variations in turbulent mixing rates and temperature in the BBL (Fig. 4b,c).

A closer look at such variability during a typical 24-h period in May (16 May 2018) is shown in Fig. 5. Methane flux sampling occurred on this date from 10:00 to 13:00 (dashed vertical black lines, Fig. 5). On this date, temperature and stratification fluctuated through the seiche period (Fig. 5a,b). Temperature fluctuations were small (< 0.07°C), and their relationship with seiche-induced velocities was complex. For example, small temperature increases were observed at 04:00 and 17:00 (Fig. 5a) as the flow transitioned from up-lake to down-lake (Fig. 5c), but the largest temperature increase was observed during the $CH_4$ sampling period, as flow transitioned from down-lake to up-lake at 10:30. Temperatures varied with elevation, leading to fluctuations in stratification as measured by buoyancy frequency $N$ (Fig. 5b). For example, near-bed cooling occurred during the latter half of $CH_4$ sampling. During this period, temperatures first dropped below 8.3°C at measurement elevation $z = 0.18$ m above the lakebed (11 : 45), and subsequently at increasingly higher elevations (by 12:15 at $z = 0.46$ m, and by 13:45 at $z = 0.86$ m). The initial appearance of cold water near the bed at 11:45 generated intense stratification (Fig. 5b), which propagated upward through the BBL as temperatures subsequently dropped at higher elevations. This pattern could be explained by upward mixing of colder water from below the lowest temperature logger ($z = 0.18$ m), or by propagation of a tilted cold front past the measurement location.

Along-lake velocities exceeded across-lake velocities (Fig. 5c,d). Intervals of relatively high (≥ 0.02 m $s^{-1}$) velocities from the seiche stimulated intense viscous dissipation of turbulent energy, particularly near the bed (Fig. 5e). For example, from 04:00 to 09:00, a period of down-lake flow (positive $u$, flowing towards the reservoir outlet; Fig. 5c) corresponded with large turbulent
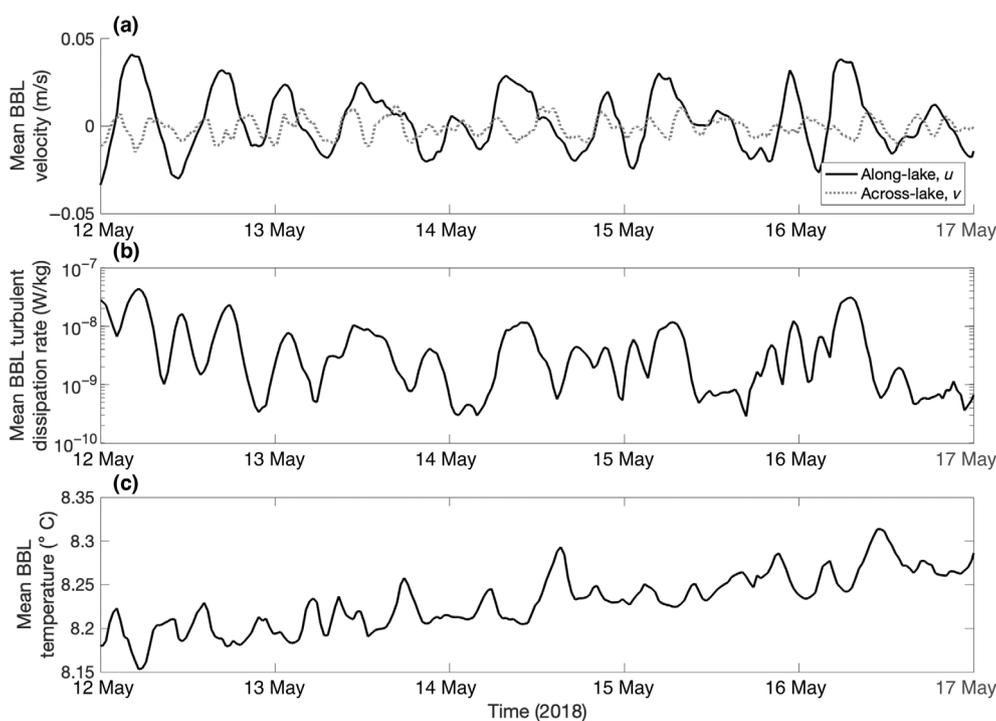
**Fig. 4.** Half-hourly averages of the mean (**a**) along-lake velocity ($u$; black line) and across-lake ($v$; dotted gray line) velocity; (**b**) turbulent dissipation rate ($\varepsilon$); and (**c**) temperature in the bottom meter of Lacamas for a representative 5-d period in May. Positive and negative $u$ indicate down-lake and up-lake flows, respectively.

dissipation rates throughout the BBL (up to $\mathcal{E} = 10^{-7}$ W kg$^{-1}$; Fig. 5e). After 11:00, flows were generally weaker, and turbulent dissipation less intense. However, an interval of weak up-lake flow (negative $u$, flowing towards the reservoir inlet) during the latter half of the CH$_4$ flux sampling period coincided with moderate turbulent dissipation near the bed (up to $\mathcal{E} = 10^{-8}$ W kg$^{-1}$ below $z = 0.4$ m from about 11:40 to 14:00).

Consistent with previous observations (Lorke et al. 2003; Bryant et al. 2010; Schwefel et al. 2017), seiche-induced changes in BBL turbulent dissipation caused substantial variations in the estimated thickness of the viscous and diffusive sublayers. Estimated diffusive sublayer thickness ranged from 0.08 to 0.4 cm and viscous sublayer thickness ranged from 0.9 to 5.0 cm (Fig. 5f). Since the diffusive sublayer can limit chemical fluxes between sediments and overlying waters, thinner sublayers can lead to periods of relatively rapid transport across the sediment–water interface (Lorke et al. 2003; Bierlein et al. 2017). Thin sublayers were observed during periods of fast flows and intense turbulent dissipation, such as 04:00–09:00 (Fig. 5c). Similarly, sublayers thinned during the last half of the CH$_4$ sampling interval, as velocity increased and moderate turbulent dissipation rates developed near the bed.

During intervals of weak flow, density stratification often strongly inhibited turbulent mixing, as indicated by Ri$_g$ values greater than 0.25 (Fig. 5g; Miles 1961). During such times, Re$_b$ values occasionally dropped below 25 (Fig. 5h), suggesting

that even the largest (Ozmidov-scale) eddies were strongly dissipated by viscosity, possibly leading to a collapse of turbulent mixing (Stillinger et al. 1983). In contrast, during intervals of strong flow, stratification was too weak to have a large local effect on turbulent mixing, as indicated by Ri$_g$ <0.05. During such times, much larger Re$_b$ indicated active turbulent mixing. Consistent with previous observations in Lacamas (Henderson 2016a), strong inhibition of turbulent mixing by stratification (i.e., Ri$_g$ >0.25) was more common in the outer BBL than the inner BBL.

The fluctuations in turbulent mixing, stratification, and temperatures described above influenced turbulent diffusivity (and thus piston velocities, Eq. 8) during the 3 h of CH$_4$ flux sampling on 16 May 2018, as shown in Figs. 5i, 6. As outlined above, during the latter half of CH$_4$ flux sampling, turbulent dissipation rates increased below $z = 0.4$ m and corresponding diffusive and viscous sublayer thickness decreased (Fig. 5e,f). Simultaneously, turbulent diffusivity also increased below $z = 0.4$ m during the latter half of CH$_4$ flux sampling (Fig. 6a), suggesting faster transport across the sediment–water interface into the inner BBL. However, owing to evolving stratification (Fig. 5b), turbulent diffusivity did not increase at $z = 0.4$ m and above during the same interval. Consequently, piston velocities representing layer-integrated mixing in the inner BBL remained relatively constant during this period, whereas piston velocities in the outer BBL decreased throughout sampling (Fig. 6b).
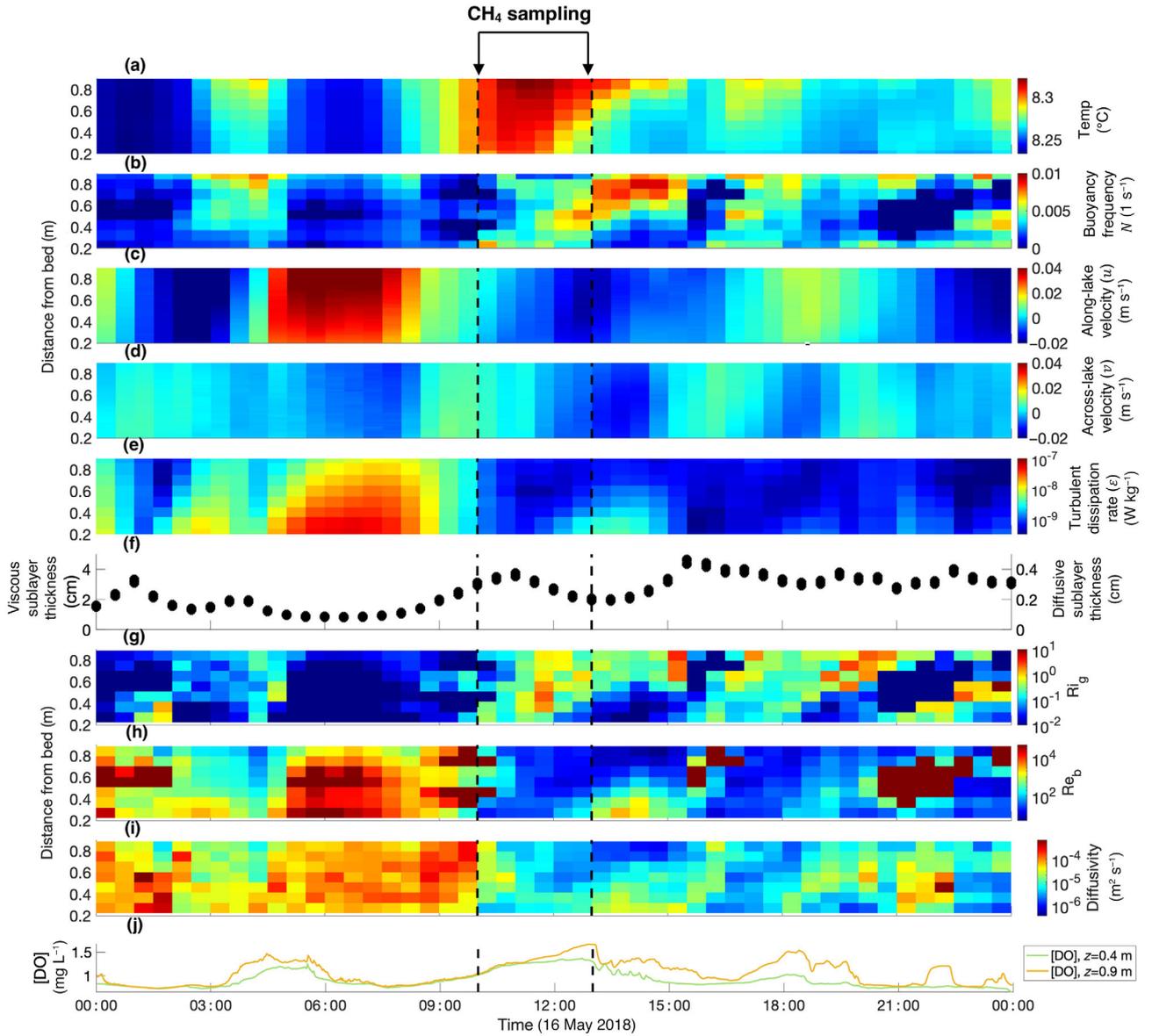
**Fig. 5.** Conditions in the BBL during 24 h on 16 May 2018. Vertical black dashed lines denote start and end of CH$_4$ sampling on this date (*see* Fig. 7). (**a**) Temperature by height in the BBL; (**b**) buoyancy frequency ($N$); (**c**) along-lake velocity ($u$, Fig. 2), with positive and negative velocities indicating down-lake and up-lake flows, respectively; (**d**) across-lake velocity ($v$, Fig. 2); (**e**) turbulent dissipation rate ($\varepsilon$); (**f**) thickness of the viscous sublayer ($\delta_v$) and diffusive sublayer ($\delta_d$) in the BBL; (**g**) gradient Richardson numbers (Ri$_g$); (**h**) buoyancy Reynolds number (Re$_b$); (**i**) turbulent diffusivity; and (**j**) DO concentrations measured at $z = 0.4$ m (green line) and $z = 0.9$ m (orange line) above the bed. All panels present half-hourly averages except for panel (**j**), which shows DO measured once per minute.

## Sub-daily CH$_4$ and DO dynamics

In spring, prior to the onset of summer anoxia, the seiche was responsible for substantial variability in DO concentrations in the BBL (Fig. 5j). High DO concentrations were generally observed where temperatures were warmer, whereas lower concentrations were observed where temperatures were cooler. For example, during CH$_4$ flux sampling on 16 May 2018, DO increased at $z = 0.4$ and $z = 0.9$ m (Fig. 5j) as measured temperatures increased at the same elevations (Fig. 5a). This correlation between temperature and DO is expected as warmer

water arriving to the BBL has been moved down from a shallower part of the water column, nearer to regions of photosynthesis and atmospheric exchange.

Methane concentrations measured at three elevations in the BBL ($z = 0.1$, 0.4, and 0.9 m) also exhibited sub-daily variations (Fig. 6c). During the periods of most rapid variability, CH$_4$ concentrations could change twofold to threefold within several hours. Regardless of fluctuations, CH$_4$ concentrations were usually larger at sampling elevations closer to the sediments than farther away from sediments, resulting
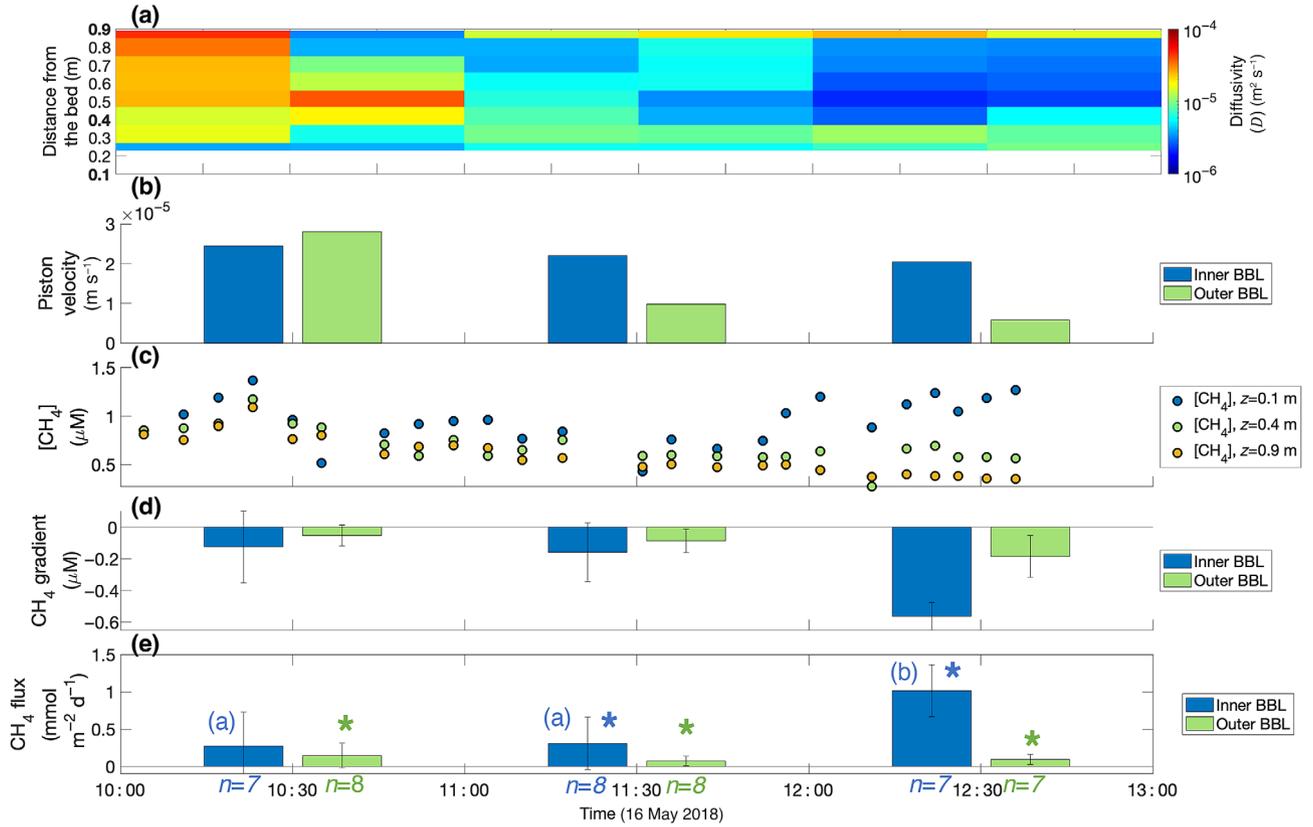
**Fig. 6.** Conditions in the BBL on 16 May 2018 during the $CH_4$ sampling period. (**a**) Half-hourly averages of turbulent diffusivity, with bolded tick labels on $y$-axis indicating elevations above the bed at which $CH_4$ concentrations were measured; (**b**) hourly average piston velocity; (**c**) $CH_4$ concentrations measured every 5–10 min at $z = 0.1$ m (blue points), $z = 0.4$ m (green points), and $z = 0.9$ m (yellow points); (**d**) hourly average $CH_4$ gradients ($\pm$ 1 standard deviation); and (**e**) hourly average $CH_4$ flux ($\pm$ 1 standard deviation). In (**b,d,e**), blue and green bars represent values measured across the inner BBL ($z = 0.1$–0.4 m above the bed) and outer BBL ($z = 0.4$–0.9 m), respectively. Asterisks in plot (**e**) indicate fluxes significantly different from zero by one-sample $t$-test or Wilcoxon rank sum test, $p < 0.05$. Letters in plot (**e**) indicate statistically significant groupings of fluxes (Kruskal–Wallis test, $p < 0.05$) and $n$ values indicate sample size per hour.

in consistently negative mean $CH_4$ gradients ($C_{z_2} - C_{z_1} < 0$, Fig. 6d) and therefore positive (upward) flux in the inner and outer BBL (Fig. 6e).

On 16 May 2018, $CH_4$ gradients were small and variable throughout the first 2 h of sampling (Fig. 6d). In the last hour of sampling, $CH_4$ gradients increased by almost fourfold in the inner BBL ($-0.59 \pm 0.09$ $\mu$M) and more than doubled in the outer BBL ($-0.19 \pm 0.13$ $\mu$M). The large increase in inner BBL $CH_4$ gradients resulted from a rapid increase in $CH_4$ concentration at $z = 0.1$ m, which reached values exceeding 1 $\mu$M, coinciding with the arrival of relatively cold water at the same elevation (Fig. 5a). In contrast, the more modest increase in outer BBL $CH_4$ gradients resulted from a slight decrease in $CH_4$ concentrations at $z = 0.9$ m and little change at $z = 0.4$ m.

## Sub-daily $CH_4$ flux magnitude and variability

Estimated methane fluxes in the inner and outer BBL fluctuated over hourly time scales. Periods of persistent $CH_4$ gradients and upward fluxes were interspersed with periods of weak gradients and fluxes small enough be statistically

indistinguishable from zero. For example, on 16 May 2018, $CH_4$ fluxes in the inner BBL were small and variable enough during the 1st hour of sampling to be statistically insignificant, whereas inner BBL fluxes in the 2nd and 3rd hours of sampling were statistically significant (Fig. 6e). In the 3rd hour of sampling, inner BBL fluxes increased by more than fourfold. This increase was driven by a larger $CH_4$ gradient (Fig. 6d) rather than a change in piston velocities, which were relatively constant during this interval in the inner BBL (Fig. 6b). In the outer BBL, gradients were less variable and fluxes were statistically significant during all 3 h of sampling.

Most fluxes observed in the BBL were positive. Across $n = 12$ total hours of flux sampling in 2018, upward $CH_4$ fluxes were observed during $n = 10$ h in the inner and outer BBL. Statistically significant fluxes were observed during $n = 6$ out of $n = 12$ total sampling hours in the inner and outer BBL, all of which were upwards fluxes. During the remaining $n = 6$ out of $n = 12$ sampling hours in 2018, statistically insignificant fluxes were measured in the inner and outer BBL, coinciding with periods of weak $CH_4$ gradients. Rarely, brief

periods of very small, negative (downward) flux were observed ($n = 2$ h in the inner and outer BBL in 2018) when $CH_4$ gradients were weak enough to reverse in sign ($C_{z_2} - C_{z_1} > 0$). Methane gradients and piston velocities were generally weaker in the outer BBL (Fig. 6b,d), resulting in generally smaller outer BBL fluxes compared with inner BBL fluxes (Fig. 6e).

### Seasonal mixing and stratification

Seasonal trends in BBL dynamics and $CH_4$ fluxes were examined during from May to August 2017. Thermal stratification developed in the full water column of Lacamas during the transition from spring to summer (Fig. 7a). Prior to May, the water column was relatively well mixed, with temperatures ranging between 9 and 11°C. The thermocline, defined as the depth of the steepest temperature gradient, first developed at a depth of about 1 m between sampling dates 28 April 2017 and 03 May 2017 (black arrows, Fig. 7a). The thermocline deepened gradually from early May to mid-July, then stabilized at about 4–5 m depth and separated the warmer epilimnion (20–25°C) from the colder hypolimnion
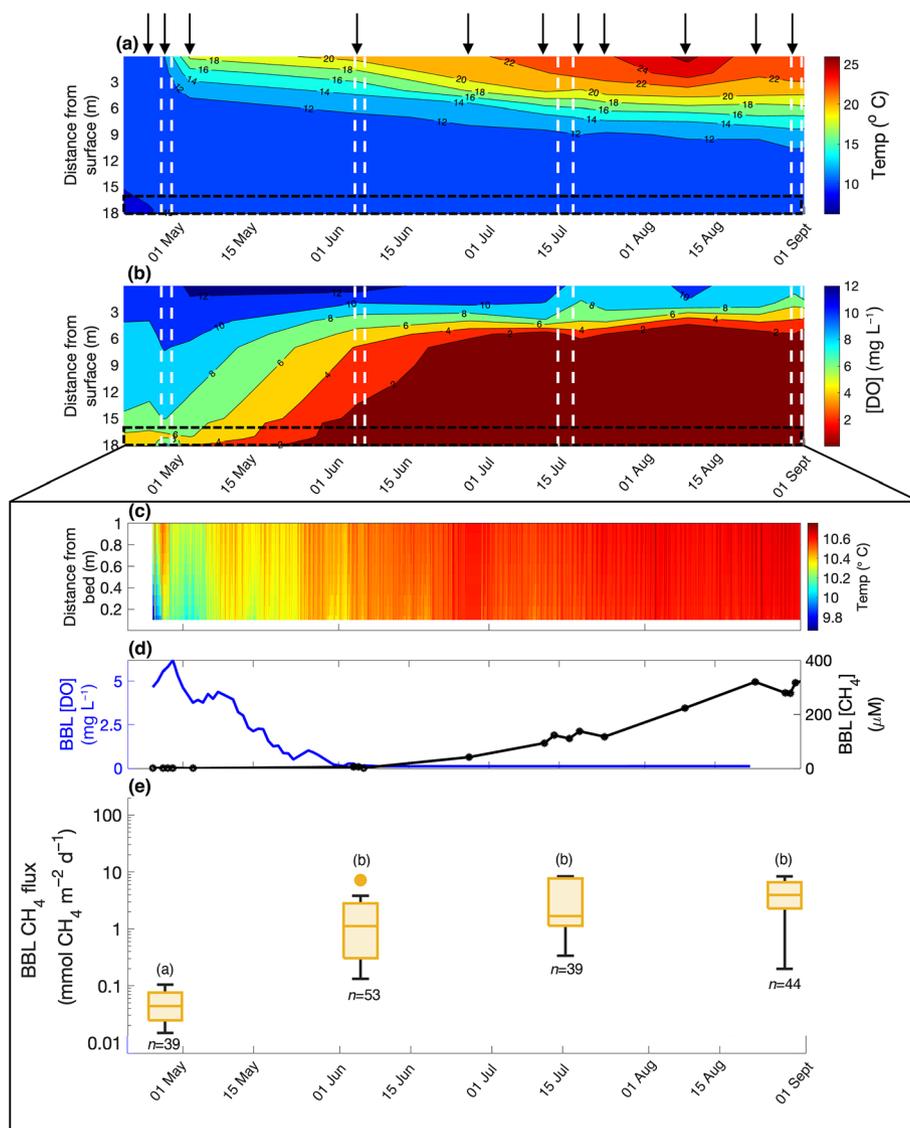


**Fig. 7.** Time series of conditions in full water column (top panel) and BBL specifically (inset) during spring and summer 2017. (**a**) Temperature in the full water column. Black contour lines for every 2°C shown. (**b**) DO concentrations in the full water column. Black contour lines for every 2 mg L⁻¹ shown. Black arrows at the top of the figure indicate sampling dates of temperature (**a**) and oxygen (**b**) in the full water column, with measurements interpolated in between dates. White dashed vertical lines indicate sampling dates for $CH_4$ fluxes in the BBL. (**c**) Temperature in the BBL averaged half-hourly. (**d**) Mean $CH_4$ concentrations (black line, measured 2–4 times per month) and daily mean DO (blue line) concentrations in the BBL. (**e**) $CH_4$ fluxes measured from $z = 0.1$ to 0.9 m above the bed and averaged hourly. Each box in (**e**) pools data from two sampling dates in the same month. Number of $CH_4$ gradient observations shown below each box and statistically significant groupings indicated with letters above each box (Kruskal–Wallis test and Dunn's post hoc, $p < 0.01$).

(10–15°C) for the remainder of sampling. Within the BBL specifically, mean daily temperatures gradually warmed starting in April (9.8°C) and stabilized around 10.6°C from July to September (Fig. 7c).

### Seasonal CH$_4$ and DO dynamics

The development of thermal stratification in the water column coincided with O$_2$ depletion and CH$_4$ accumulation in the BBL and hypolimnion (Fig. 7b,d). Note that full water column data presented in panels Fig. 7a,b are interpolated over bimonthly sampling dates (*see* Fig. 7 caption). Nevertheless, the summertime trend towards increasing stratification and reduced hypolimnion O$_2$ concentrations is clear, and rapid near-bed sampling provided much higher resolution of BBL temperatures used for CH$_4$ flux calculations (*see* "Methods" section). Daily DO concentrations in the BBL, averaged between measurements at $z = 0.4$ and 0.9 m above the bed, dropped from over 5.0 mg L$^{-1}$ in early May to less than 0.1 mg L$^{-1}$ in early June 2017 (Fig. 7d). Conditions remained anoxic (DO < 2 mg L$^{-1}$; Nürnberg 2022) in the BBL throughout the remainder of the 2017 sampling period. The decrease in DO concentrations measured in the BBL was consistent with the development of hypoxia (DO < 5 mg L$^{-1}$; Nürnberg 2022) in the hypolimnion in June, followed by complete anoxia in the hypolimnion in July and August (Fig. 7b). CH$_4$ concentrations within the BBL started at 0.7–1.1 $\mu$M in late April 2017 (Fig. 7d; Supporting Information Table S2). Once thermal stratification was established in early June, CH$_4$ concentrations rose to 1.5–5.9 $\mu$M. Methane concentrations continued to increase steadily to 110–137 $\mu$M in mid-July and 278–317 $\mu$M in late August.

### Seasonal CH$_4$ flux magnitude and variability

Methane fluxes measured bimonthly from April to August (excluding May) showed a distinct seasonal increase after the lake stratified (Fig. 7e; Table 1). Median fluxes increased more than 100-fold, from 0.11 mmol m$^{-2}$ d$^{-1}$ in April to 36 mmol m$^{-2}$ d$^{-1}$ in August, and fluxes measured in April were significantly lower than those measured in June, July, and August (Fig. 7e). Methane fluxes were also highly variable over daily timescales, spanning one to two orders of magnitude between sampling dates 2–3 d apart (Table 1). This large flux variability between closely spaced sampling dates is expected given the sub-daily variability described above (in Fig. 6).

### Hypolimnetic CH$_4$ balance

As mixing across the metalimnion was suppressed by thermal stratification in June, July, and August 2017 (Fig. 7a), CH$_4$ accumulated in the hypolimnion (Fig. 7d; Supporting Information Table S3). The rate of CH$_4$ accumulation ranged from 0.66 mmol m$^{-2}$ d$^{-1}$ in June to 18 mmol m$^{-2}$ d$^{-1}$ in August, corresponding to a daily rate of 0.36–9.5 kmol d$^{-1}$ for the entire hypolimnion (Fig. 8). If CH$_4$ loss from the hypolimnion

**Table 1.** Average daily flux and number of flux observations for sampling dates in 2017.

| Sampling date | Number of flux observations | Average daily flux (mean $\pm$ SD; mmol m$^{-2}$ d$^{-1}$) |
|---|---|---|
| 27 Apr 2017 | 16 | 0.11 $\pm$ 0.12 |
| 29 Apr 2017 | 23 | 0.11 $\pm$ 0.09 |
| 4 Jun 2017 | 30 | 23 $\pm$ 28 |
| 6 Jun 2017 | 23 | 2.8 $\pm$ 4.6 |
| 14 Jul 2017 | 23 | 63 $\pm$ 41 |
| 17 Jul 2017 | 19 | 8.5 $\pm$ 8.5 |
| 29 Aug 2017 | 22 | 24 $\pm$ 19 |
| 31 Aug 2017 | 21 | 71 $\pm$ 48 |

via diffusion through the metalimnion and oxidation were negligible, the rate of hypolimnetic CH$_4$ accumulation would approximately balance the rate of BBL CH$_4$ flux. However, monthly time-averaged BBL fluxes (13–47 mmol m$^{-2}$ d$^{-1}$ or 1.1–25 kmol d$^{-1}$; Fig. 8) were consistently larger than observed CH$_4$ accumulation rates. Only 12–38% of CH$_4$ transported across the BBL remained stored below the metalimnion, and only 0.07–3.2% (0.0012–1.3 mmol m$^{-2}$ d$^{-1}$, or 0.00075–0.80 kmol d$^{-1}$; Fig. 8) was transferred from the hypolimnion via diffusion into the metalimnion. The remaining 58–88% of CH$_4$ transported across the BBL was presumably removed from the hypolimnion at a rate of 1.4–32 mmol m$^{-2}$ d$^{-1}$ (0.77–17 kmol d$^{-1}$; Fig. 8).

Methane oxidation in the hypolimnion was likely responsible for the bulk of CH$_4$ loss. CH$_4$ oxidation rates in June and July, measured directly using water incubations at $z = 0.9$ m, were 13–39 mmol m$^{-2}$ d$^{-1}$ and therefore sufficiently large to explain the loss. Similarly, potential oxidation rates (182 mmol m$^{-2}$ d$^{-1}$), calculated in August using a first-order rate law for methanotrophy observed in the Lacamas hypolimnion (Eq. 13) could account for more than enough CH$_4$ oxidation to balance the hypolimnion CH$_4$ budget in August. In June, enough oxygen was present in the hypolimnion (Fig. 7b) to sustain the observed CH$_4$ oxidation (Supporting Information Table S4). However, as oxygen depletion in the hypolimnion continued throughout July and August (Fig. 7b), hypolimnetic concentrations of electron acceptors commonly attributed to CH$_4$ oxidation (O$_2$, NO$_3^-$, and SO$_4^{2-}$) were insufficient to fuel the observed CH$_4$ oxidation for more than 6–8 d (Supporting Information Table S4).

## Discussion

### Comparison with other flux measurement methods

In this study, we applied a flux gradient approach to compare spatiotemporal variations in physical conditions, biogeochemical conditions, and CH$_4$ fluxes in the BBL of a lake at
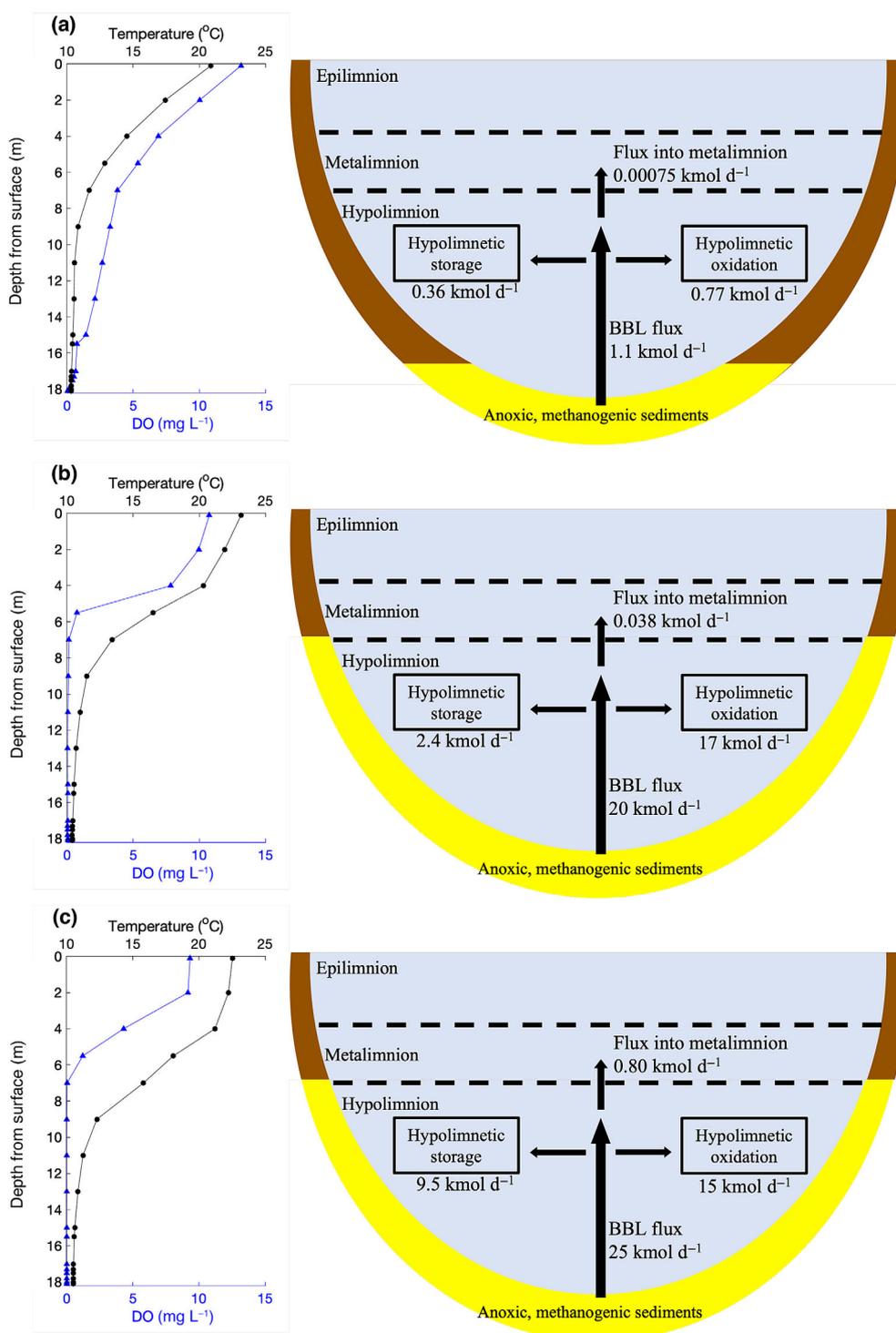
**Fig. 8.** For June (**a**), July (**b**), and August (**c**) 2017, left panels show representative temperature (black) and DO (blue) depth profiles and right panels show the calculated hypolimnetic CH$_4$ balance. In the mass balance, arrow size approximates the relative rates of transport from the BBL, hypolimnetic storage, transport to the metalimnion and hypolimnetic oxidation, yet arrows are not quantitatively to scale. Dashed lines delineate the metalimnion (4–7 m from the surface). The surface area of sediments in the full hypolimnion (7 m depth and below) was used to convert rates (mmol m$^{-2}$ d$^{-1}$) of hypolimnetic CH$_4$ storage, flux into the metalimnion, and oxidation into rates of kmol CH$_4$ d$^{-1}$. For converting time-averaged BBL flux (mmol m$^{-2}$ d$^{-1}$) into kmol CH$_4$ d$^{-1}$, only the surface area of sediments overlain by anoxic water and therefore considered to be actively producing CH$_4$ (highlighted in yellow; sediments at 17 m depth and below in June, 7 m depth and below in July and August) was used. Mass balance values rounded to two significant figures.

**Table 2.** Minimum, mean, and maximum CH$_4$ fluxes across the sediment–water interface (top rows; rates displayed in the same significant figures as reported by authors) and across the BBL from this study (bolded rows). Empty boxes indicate no data.

| Study | Method | Trophic status | Min (mmol m$^{-2}$ d$^{-1}$) | Mean (mmol m$^{-2}$ d$^{-1}$) | Max (mmol m$^{-2}$ d$^{-1}$) |
|---|---|---|---|---|---|
| Maerki et al. (2009) | Benthic chambers | Eutrophic | | 7.5 | |
| Kuivila et al. (1988) | Benthic chambers | Mesotrophic | 0.21 | | 0.31 |
| Donis et al. (2017) | Fickian diffusion model | Mesotrophic | 1.6 | | 6 |
| Steinsberger et al. (2017) | Fickian diffusion model | Multiple | 0.08 | | 4.24 |
| Carignan and Lean (1991) | Fickian diffusion model | Mesotrophic | 1 | | 5 |
| Norði et al. (2013) | Fickian diffusion model | Eutrophic | | 0.04 | |
| Huttunen et al. (2006) | Fickian diffusion model | Multiple | 0.03 | | 6.55 |
| Brand et al. (2009) | Fickian diffusion model | Eutrophic | | | 1.25 |
| Gruca-Rokosz and Tomaszek (2015) | Fickian diffusion model | Eutrophic | 0.01 | | 2.19 |
| Strayer and Tiedje (1978) | Fickian diffusion model | Hypereutrophic | 10 | 25 | 46 |
| Matthews et al. (2005) | Mass balance | Hypereutrophic | 7.3 | | 11.7 |
| Rudd and Hamilton (1978) | Mass balance | Eutrophic | 1 | | 10 |
| Kelly and Chynoweth (1980) | Mass balance | | 3.2 | | 9.8 |
| Bastviken et al. (2008) | Mass balance | Multiple | 3.87 | | 5.05 |
| Fallon et al. (1980) | Mass balance | Eutrophic | | 35.8 | |
| Peeters et al. (2019) | Mass balance | Multiple | 0.16 | 2 | 7.4 |
| Clayer et al. (2016) | Reaction-transport model | Oligotrophic | 0.104 | | 7.46 |
| **This study (Apr–Aug 2017)** | **Flux gradient** | **Eutrophic** | **0.03** | **24** | **94** |
| **This study (May 2018, inner BBL)** | **Flux gradient** | **Eutrophic** | **−2.1** | **9.6** | **85** |
| **This study (May 2018, outer BBL)** | **Flux gradient** | **Eutrophic** | **−0.58** | **2.7** | **16** |

sub-daily and seasonal time scales. Like the eddy covariance approach, the flux gradient approach yields turbulent flux estimates a small distance above the sediment–water interface. Previous eddy covariance observations suggest that vertical variability could cause BBL fluxes to differ from sediment–water fluxes, particularly over short timescales (Brand et al. 2008). However, given the proximity of the BBL to lake sediments, comparing rates of both processes is useful for understanding how CH$_4$ released from sediments is transported into the hypolimnion.

Mean CH$_4$ fluxes from the flux gradient approach (2.7–24 mmol m$^{-2}$ d$^{-1}$; Table 2), estimated on an hourly basis then averaged across sampling periods in 2017 or 2018, were similar to mean sediment–water fluxes measured in other lake systems using other methods (2–35.8 mmol m$^{-2}$ d$^{-1}$; Table 2).

Mean CH$_4$ fluxes reported here were also comparable to the mean sediment CH$_4$ production rate reported in a meta-analysis of incubation experiments across a variety of lakes and reservoirs (2.98 mmol m$^{-2}$ d$^{-1}$ mean, 0–21.8 mmol m$^{-2}$ d$^{-1}$ range; D'Ambrosio and Harrison 2021). However, compared with other approaches, the fluxes observed here were more variable and had a higher maximum. We report fluxes spanning more than three orders of magnitude (0.03–94 mmol m$^{-2}$ d$^{-1}$ in 2017), a wider range than that of sediment–water fluxes reported for all systems in the literature previously (0.01–46 mmol m$^{-2}$ d$^{-1}$). In addition, the maximum fluxes we report (up to 94 mmol m$^{-2}$ d$^{-1}$) are approximately twice as large as the highest previously reported sediment–water fluxes (up to 46 mmol m$^{-2}$ d$^{-1}$; Strayer and Tiedje 1978).

As a check on our CH$_4$ flux estimates, we estimated oxygen fluxes in the outer BBL for the time period shown in Fig. 6 using DO gradients (Fig. 5j) and the same piston velocities used for calculating CH$_4$ fluxes (Fig. 6b). Oxygen fluxes during this hypoxic period ranged from $-0.5$ to $-5$ mmol m$^{-2}$ d$^{-1}$ (negative values indicating a flux toward the bed). These values are similar to benthic oxygen fluxes observed in the BBL of Lake Lucerne throughout the seiche cycle ($-3.5$ to $-45$ mmol m$^{-2}$ d$^{-1}$; Brand et al. 2008), in the hypoxic BBL of Daheiting Reservoir (not exceeding $-1$ mmol m$^{-2}$ d$^{-1}$; Zhang et al. 2021), and in the BBL of a riverine lake ($-6.4$ to $-84$ mmol m$^{-2}$ d$^{-1}$; Murniati et al. 2015). The reasonable O$_2$ flux estimates suggest that our piston velocities (and in turn CH$_4$ fluxes) were not greatly overestimated.

A substantial component of the variability in our flux estimates resulted from seiche-induced fluctuations in mixing rates. Similarly large variability in BBL oxygen fluxes, also resulting from variations in mixing rates throughout a seiche cycle, has previously been observed using eddy covariance (Brand et al. 2008) and microprofiler measurements (Lorke et al. 2003). Typical approaches for measuring sediment–water CH$_4$ flux, such as benthic chambers, incubations, and modeling, exclude the influence of sub-daily variations in BBL mixing rates. The large range of our flux estimates suggest that incorporating the influence of fluctuating BBL mixing rates, as done here, reveals significant temporal variability in CH$_4$ transport from sediments in situ. Furthermore, the large magnitude of maximum fluxes in our study indicates that CH$_4$ transport in the BBL is likely punctuated by periods of intense flux previously unresolved by conventional methods.

The estimates of small fluxes presented here may be prone to error because they primarily occurred during periods of weak concentration gradients or minimal mixing. Occasional negative flux estimates (17% of hourly estimates in 2018, but none in 2017) resulted from reversals in concentration gradients. These reversals were most common when gradients were weak, and may have resulted from random turbulent fluctuations in concentration. Moreover, in very low-energy stratified conditions, with Re$_b$ < 10–25, turbulent mixing becomes intermittent and difficult to measure (Stillinger et al. 1983; Ivey and Imberger 1991), so that associated flux estimates are prone to large relative errors. However, such low-Re$_b$ periods were infrequent, with an hourly average Re$_b$ <25 present during just 12% of CH$_4$ sampling hours in 2017 and 16% of hours in 2018. Moreover, fluxes observed during low-Re$_b$ times were uniformly small and contributed only 2–13% to the total integrated flux on each sampling date. Therefore, time-averaged fluxes are likely insensitive to even substantial relative errors in estimates of fluxes occurring during low-Re$_b$ times.

### Sub-daily controls on fluxes

Estimated CH$_4$ fluxes showed major variability over time-scales of several hours. An example from 1 day is shown in Fig. 6, and similar variability was observed during the majority of sampling days. Multiple physical and biological factors, such as lateral advection, fluctuations in methanotrophy within the BBL, and/or seiche-induced variations in turbulent mixing, could have interacted to produce the temporal changes in flux observed in Fig. 6e. We examine each possible driver individually below and suggest that seiche-induced fluctuations in turbulent mixing, rather than fluctuations in lateral advection or methanotrophy, were an important control on fluxes in the time series shown in Fig. 6.

Lateral advection of CH$_4$ in or out of the sampled region of the BBL may have influenced CH$_4$ gradient and flux estimates. For the case shown in Fig. 6, the increase in CH$_4$ concentration at $z = 0.1$ m above the bed (Fig. 6c) coincided with a decrease in temperature at the same elevation (Fig. 5a), as would be expected if the seiche advected CH$_4$-rich cold water over the measurement location. The lack of simultaneous increase in temperature and CH$_4$ concentration at $z = 0.4$ m, which led to the increased CH$_4$ gradient and flux, could be explained if a tilted cold front propagated over the measurement location. However, this explanation is called into question by the fact that the CH$_4$ concentration at $z = 0.4$ m did not rise when the cold water finally arrived at $z = 0.4$ m during the third hour of sampling. More generally, if CH$_4$, like temperature, were transported as a passive tracer without local sources or sinks, then a strong correlation between temperature gradients and CH$_4$ gradients would be expected. Across all sampling days, a lack of correlation between temperature gradients and CH$_4$ gradients (Supporting Information Fig. S1) suggests that lateral advection was not the most important driver of CH$_4$ dynamics in the near-bed region measured here.

Methanotrophic activity in the water column could also influence CH$_4$ flux estimates by consuming CH$_4$ within the sampled region of the BBL. For example, oxidation of CH$_4$ might explain the consistent trend of greater fluxes observed in the inner BBL compared to the outer BBL (Fig. 6e). If this was the case, BBL oxidation would approximately balance the flux difference observed between the inner and outer BBL ($R_{ox-BBL} = F_{inner} - F_{outer}$). In order to evaluate the potential importance of within-BBL oxidation, we estimated hourly, depth-integrated oxidation rates in the BBL ($R_{ox-BBL}$) during the time series presented in Fig. 6 by applying and vertically integrating Eq. 13 from $z = 0.25$ to $z = 0.65$ m above the bed:

$$R_{ox-BBL} = \int_{z=0.25}^{z=0.65} mC dz, \qquad (14)$$

where the integral was evaluated by linearly interpolating the CH$_4$ concentration $C$ between measurement elevations. The ratio of $R_{ox-BBL}$ to the difference in fluxes between the inner and outer BBL ($F_{inner} - F_{outer}$) was typically 0.01–0.1, suggesting that within-BBL oxidation could only explain

1–10% of the flux difference in the inner and outer BBL during the time shown in Fig. 6. This is a high-end estimate of the potential role of CH$_4$ oxidation, because oxidation rates estimated with Eq. 13 are likely closer to potential rates than actual rates (*see* "Methods" section). Therefore, when only methanotrophy occurring within the thin BBL is considered, consumption was likely too slow to explain the observed variability in BBL fluxes with elevation. However, when methanotrophy occurring throughout the much larger region of the entire hypolimnion is considered, total consumption does appear sufficient to influence CH$_4$ dynamics (Fig. 8).

Our results suggest that seiche-induced variation in turbulent mixing within the BBL, rather than changes in lateral advection or water column methanotrophy, was likely responsible for the short-term variability shown in Fig. 6e. We hypothesize that methane may accumulate near the bed during periods of weak mixing, and subsequently flux upwards past our measurement locations only when turbulent mixing increases. This may explain the observed increase in inner BBL CH$_4$ fluxes observed during the last hour of sampling on 16 May 2018 (12:00–13:00; Fig. 6e). Consistent with this hypothesis, the inner BBL flux increase was a consequence of greater CH$_4$ concentrations at $z = 0.1$ m (Fig. 6c), which steepened the CH$_4$ gradient (Fig. 6d). Methane concentrations at higher elevations did not decrease during the same period (Fig. 6c), as would be expected if loss of CH$_4$—either through lateral advection or oxidation—was responsible for the steeper gradient and larger flux observed in the last hour of sampling (Fig. 6d,e). Rather, we observed greater near-bed mixing during this last hour, quantified by a reduced thicknesses of diffusive and viscous sublayers (Fig. 5f). Therefore, we attribute the increase in flux from 12:00 to 13:00 to episodically elevated upward transport of CH$_4$ accumulated near the bed, rather than lateral advection or methanotrophy.

Changes in methanotrophy and/or methanogenesis within the surface sediment could also play a role in sub-daily CH$_4$ flux variations observed in the BBL. For example, temporal variations in oxygen availability at the sediment–water interface could influence the activity of surface sediment methanogens, which are highly sensitive to DO concentrations (Borrel et al. 2011). Variations in the concentration of oxygen or other electron acceptors could similarly affect methanotrophic activity within the surface sediment (Martinez-Cruz et al. 2018). However, we did not monitor sediment microbial communities during our study; therefore, we cannot exclude variations in sediment microbial activity as a potential control on sub-daily CH$_4$ dynamics.

### Seasonal controls on fluxes

The wide range of fluxes in our study was in part due to the seasonal increase in CH$_4$ fluxes observed from spring to summer 2017 (Fig. 7e; Table 1). This increase may have resulted from the development of hypolimnetic hypoxia, and then anoxia, as the full water column of Lacamas thermally

stratified (Fig. 7a,b). Development of BBL anoxia (Fig. 7d) likely coincided with a depletion of oxygen within the surface sediment, possibly facilitating increased methanogenic activity close to the sediment–water interface (Frenzel et al. 1990; Liikanen et al. 2003; Huttunen et al. 2006). Furthermore, the transition through hypoxic to anoxic conditions in the hypolimnion (Fig. 7b) may have suppressed aerobic CH$_4$ oxidation in the surface sediment (Frenzel et al. 1990). Elevated surface chlorophyll *a* concentrations (Perkins et al. 2019) may have also stimulated CH$_4$ production by increasing the supply of carbon to sediments (West et al. 2012; Rodriguez et al. 2018). Lastly, temperature also influences CH$_4$ fluxes. In laboratory experiments, increasing sediment temperatures by 6–26°C stimulated CH$_4$ production rates by 10- to 100-fold (Duc et al. 2010). However, since temperatures observed 0.1 m above the bed increased less than 1°C from spring to summer in Lacamas (Fig. 7c), the temperature dependence of methanogenesis could not explain the 100-fold increase in fluxes observed from April to August in our study (Fig. 7e).

### Linking CH$_4$ transport across the BBL to hypolimnion accumulation

Detailed CH$_4$ flux estimates in the BBL were time-averaged to determine the lakewide supply of CH$_4$ to the lake hypolimnion (*see* "Methods" section). The majority (58–88%) of CH$_4$ flux across the BBL appears to have been oxidized in the hypolimnion of Lacamas (Fig. 8). Much (12–38%) of the remaining CH$_4$ accumulated in the hypolimnion and a small amount (0.07–3.2%) diffused across the metalimnion to the epilimnion. These results are consistent with other studies of stratified lakes with anoxic hypolimnia, which show that most CH$_4$ diffusing out of profundal sediments is consumed before reaching the lake surface (Bastviken et al. 2008; Donis et al. 2017; Li et al. 2021). In Peter, Paul, and Hummingbird Lakes, 20–45% of CH$_4$ released from deep sediments was stored in the water column and 51–80% was oxidized, primarily in the anoxic hypolimnion (Bastviken et al. 2008). A recent study of several Siberian lakes concluded 61–100% of the upwards flux of CH$_4$ was oxidized anaerobically in the water column (Cabrol et al. 2020). Similarly, in Dendre Lake, 70–83% of the upwards flux of CH$_4$ was oxidized in the mostly anoxic water column (Roland et al. 2017).

Calculated Lake numbers (Deemer and Harrison 2019) and Wedderburn numbers (Supporting Information Table S5) suggest that maximum wind speeds were sufficient to cause occasional overturning in May and early June, likely supplying some oxygen or other electron acceptors to the hypolimnion. However, the supply of electron acceptors to the hypolimnion was greatly limited as anoxic conditions developed during July and August. Lake numbers and Wedderburn numbers increased in July and August (Supporting Information Table S5), suggesting that overturning was inhibited as summertime stratification developed. Direct measurements of along-lake temperature sections during summer confirm that

vertical isotherm displacements are small compared with the lake depth (Henderson and Deemer 2012). Consistent with these observations, time series measured at both ends of the lake during summer display seiche-induced temperature fluctuations that are much smaller than the full-depth temperature variations (Nielson and Henderson unpubl.; Deemer et al. 2015; Henderson 2016*b*).

Sufficient O$_2$ was present in the hypolimnion to explain the observed oxidation rates in June (Supporting Information Table S4). In contrast, during the July–August period of strong stable stratification, the supply of electron acceptors commonly attributed to CH$_4$ oxidation (O$_2$, NO$_3^-$, and SO$_4^{2-}$) was insufficient to fuel all of the CH$_4$ oxidation necessary to balance the hypolimnion CH$_4$ budget (Supporting Information Table S4). Therefore, although our mass balance indicates CH$_4$ oxidation was active in the lake hypolimnion during summer, it remains unclear which electron acceptors were responsible for CH$_4$ oxidation. Previous investigations in other lakes (including Lacamas) have reported significant CH$_4$ oxidation occurring in the anaerobic hypolimnion that could not be sustained by the standing supply of terminal electron acceptors available (Crowe et al. 2011; Norði et al. 2013; Blees et al. 2014; Reed et al. 2017). These studies have proposed alternative mechanisms to explain oxidation in the anaerobic hypolimnion, such as cryptic cycling of terminal electron acceptors (Norði et al. 2013), recycling of electron acceptors in the water column (Crowe et al. 2011), or micro-aerobic oxidation (Blees et al. 2014). Previous work in Lacamas has hypothesized that organic acids, possibly acting as direct electron acceptors or electron shuttles, could support significant rates of oxidation in the anaerobic hypolimnion (Reed et al. 2017). Although we do not have the data to fully explore the role of cryptic cycling, electron acceptor recycling, micro-aerobic oxidation, and/or organic acids in supporting methanotrophy within Lacamas, investigating these possible mechanisms is an important area for future work.

In our mass balance, methanotrophy was invoked to explain the mass of CH$_4$ remaining after quantifying CH$_4$ that entered, was stored, and exited the hypolimnion (Fig. 8). Accordingly, if the mass of CH$_4$ entering the hypolimnion (i.e., time-averaged fluxes across the BBL) was overestimated, hypolimnetic oxidation rates would also be overestimated. A reduction in time-averaged BBL fluxes of 68%, 88%, and 58% would be required to calculate zero oxidation in the hypolimnion in June, July, and August, respectively. If BBL fluxes were consistently overestimated by half, oxidation in the hypolimnion would still be required to explain the fate of 37%, 75%, and 17% of CH$_4$ flux observed across the BBL in June, July, and August, respectively. Our conclusion that methanotrophy is likely responsible for the loss of CH$_4$ in the hypolimnion is therefore robust even to significant overestimations of BBL flux.

Spatial variability in sediment CH$_4$ flux within Lacamas could have also contributed to error in BBL fluxes used in the mass balance. We account for some of this spatial variability in our mass balance by considering how the onset of anoxia varies with depth in the summer, influencing the surface area of sediment that releases CH$_4$ (*see* Fig. 8 and caption). Spatial variability in sediment organic carbon accumulation, which we did not consider in our study, may influence the exchange of CH$_4$, O$_2$, and other compounds between the sediment and water column (Steinsberger et al. 2017; Schwefel et al. 2018). However, considering spatial variability in sediment dynamics would likely increase our BBL flux estimates. Methane fluxes were estimated in the deepest region of the reservoir (Fig. 2), where CH$_4$ ebullition data in Lacamas suggests rates of sediment methanogenesis are low compared to shallower regions closer to the reservoir inlet (Harrison et al. 2017).

## Conclusions and future directions

The flux gradient approach, adapted here for the first time for use in a stratified lake BBL, lends new insight into patterns and controls of lake BBL CH$_4$ fluxes. Using this technique, we demonstrate large seasonal and sub-daily variability in CH$_4$ fluxes within the BBL of a seiche-driven, eutrophic reservoir. Methane transport across the BBL increased from spring to summer, coincident with the development of anoxia in the hypolimnion. Short-term fluctuations in CH$_4$ flux were linked to seiche-associated variations in BBL conditions, with smaller fluxes observed during near-bed stratification and much larger fluxes observed during bursts of intense near-bed turbulent mixing.

The implications of the observed variability in CH$_4$ fluxes are not yet well understood and an important area for future study in other seiche-driven lakes. Short-term variability in CH$_4$ transport across the BBL could potentially influence CH$_4$ supply to methanotrophs in the hypolimnion, thereby affecting a critical pathway for lentic carbon processing (Reis et al. 2022) and a significant player in the pelagic food web of some lakes (Kankaala et al. 2006*a*,*b*). Seasonal variability in BBL fluxes compared with seasonal CH$_4$ accumulation suggested intense oxidation in the anoxic hypolimnion of Lacamas, a phenomenon reported in other stratified lakes (Bastviken et al. 2008; Roland et al. 2017; Cabrol et al. 2020). Future work could identify which electron acceptors support methanotrophy in the hypolimnion, and mechanisms supporting electron transfer.

Our results also highlight the need to develop techniques that consider BBL dynamics when measuring benthic CH$_4$ fluxes (D'Ambrosio and Harrison 2022). In addition to the flux gradient approach presented here, eddy correlation (Lorrai et al. 2010) or relaxed eddy accumulation techniques (Lemaire et al. 2017) consider boundary layer dynamics and could be adapted for measuring near-bed CH$_4$ fluxes in lakes, pending the development of sufficiently high-frequency dissolved CH$_4$ sensors. Flux gradient approaches have the advantage of not requiring fast-response concentration measurements, unlike eddy covariance techniques. Therefore, the flux gradient

approach developed here could be applied to examine benthic fluxes of other ecologically important solutes that are difficult to measure with fast-response instruments, such as phosphorus or manganese. Coupling flux gradient measurements with monitoring of BBL conditions could provide potentially powerful future insight into how physical and biological processes influence the biogeochemistry of lake BBLs.

**Data availability statement**

All data are available upon request to the authors.

# References

Bastviken, D. 2009. Methane, p. 783–805. *In* Encyclopedia of inland waters. Academic Press.

Bastviken, D., J. J. Cole, M. L. Pace, and M. C. Van de-Bogert. 2008. Fates of methane from different lake habitats: Connecting whole-lake budgets and $CH_4$ emissions. J. Geophys. Res. Biogeo. **113**: 1–13. doi:10.1029/2007JG000608

Bierlein, K. A., M. Rezvani, S. A. Socolofsky, L. D. Bryant, A. Wüest, and J. C. Little. 2017. Increased sediment oxygen flux in lakes and reservoirs: The impact of hypolimnetic oxygenation. Water Resour. Res. **53**: 4876–4890. doi:10.1002/2016WR019850

Blees, J., H. Niemann, C. B. Wenk, and others. 2014. Micro-aerobic bacterial methane oxidation in the chemocline and anoxic water column of deep south-Alpine Lake Lugano (Switzerland). Limnol. Oceanogr. **59**: 311–324. doi:10.4319/lo.2014.59.2.0311, 2

Borrel, G., D. Jézéquel, C. Biderre-Petit, N. Morel-Desrosiers, J. P. Morel, P. Peyret, G. Fonty, and A. C. Lehours. 2011. Production and consumption of methane in freshwater lake ecosystems. Res. Microbiol. **162**: 833–847. doi:10.1016/j.resmic.2011.06.004

Brand, A., D. F. McGinnis, B. Wehrli, and A. Wüest. 2008. Intermittent oxygen flux from the interior into the bottom boundary of lakes as observed by eddy correlation. Limnol. Oceanogr. **53**: 1997–2006.

Brand, A., C. Dinkel, and B. Wehrli. 2009. Influence of the diffusive boundary layer on solute dynamics in the sediments of a seiche-driven lake: A model study. J. Geophys. Res. Biogeo. **114**: 1–12. doi:10.1029/2008JG000755

Bryant, L. D., C. Lorrai, D. F. McGinnis, A. Brand, A. W. Est, and J. C. Little. 2010. Variable sediment oxygen uptake in response to dynamic forcing. Limnol. Oceanogr. **55**: 950–964. doi:10.4319/lo.2010.55.2.0950

Cabrol, L., and others. 2020. Anaerobic oxidation of methane and associated microbiome in anoxic water of Northwestern Siberian lakes. Sci. Total Environ. **736**: 139588. doi:10.1016/j.scitotenv.2020.139588

Carignan, R., and D. R. S. Lean. (1991). Regeneration of dissolved substances in a seasonally anoxic lake: The relative importance of processes occurring in the water column and in the sediments. Limnol. Oceanogr. **36**: 683–707. Portico. https://doi.org/10.4319/lo.1991.36.4.0683

Crowe, S. A., and others. 2011. The methane cycle in ferruginous Lake Matano. Geobiology **9**: 61–78. doi:10.1111/j.1472-4669.2010.00257.x

D'Ambrosio, S. L., and J. A. Harrison. 2021. Methanogenesis exceeds $CH_4$ consumption in eutrophic lake sediments. Limnol. Oceanogr. Lett. **6**: 173–181. doi:10.1002/lol2.10192

D'Ambrosio, S. L., and J. A. Harrison. 2022. Measuring $CH_4$ fluxes from lake and reservoir sediments: Methodologies and needs. Front. Environ. Sci. **10**: 1–19. doi:10.3389/fenvs.2022.850070

Deemer, B. R., and J. A. Harrison. 2019. Summer redox dynamics in a eutrophic reservoir and sensitivity to a summer's end drawdown event. Ecosystems **22**: 1618–1632. doi:10.1007/s10021-019-00362-0

Deemer, B. R., J. A. Harrison, and E. W. Whitling. 2011. Microbial dinitrogen and nitrous oxide production in a small eutrophic reservoir: An in situ approach to quantifying hypolimnetic process rates. Limnol. Oceanogr. **56**: 1189–1199. doi:10.4319/lo.2011.56.4.1189

Deemer, B. R., S. M. Henderson, and J. A. Harrison. 2015. Chemical mixing in the bottom boundary layer of a eutrophic reservoir: The effects of internal seiching on nitrogen dynamics. Limnol. Oceanogr. **60**: 1642–1655. doi:10.1002/lno.10125

Deemer, B., J. Harrison, S. Li, and others. 2016. Greenhouse gas emissions from reservoir water surfaces: A new global synthesis. Bioscience **66**: 949–964, 11.

Donis, D., S. Flury, A. Stöckli, J. E. Spangenberg, D. Vachon, and D. F. McGinnis. 2017. Full-scale evaluation of methane production under oxic conditions in a mesotrophic lake. Nat. Commun. **8**: 1661. doi:10.1038/s41467-017-01648-4

Duc, N. T., P. Crill, and D. Bastviken. 2010. Implications of temperature and sediment characteristics on methane formation and oxidation in lake sediments. Biogeochemistry **100**: 185–196. doi:10.1007/s10533-010-9415-8

Eckert, W., and R. Conrad. 2007. Sulfide and methane evolution in the hypolimnion of a subtropical lake: A three-year study. Biogeochemistry **82**: 67–76. doi:10.1007/s10533-006-9053-3

Encinas Fernández, J., F. Peeters, and H. Hofmann. 2014. Importance of the autumn overturn and anoxic conditions in the hypolimnion for the annual methane emissions from a temperate lake. Environ. Sci. Technol. **48**: 7297–7304. doi:10.1021/es4056164

Frenzel, P., B. Thebrath, and R. Conrad. 1990. Oxidation of methane in the oxic surface-layer of a deep lake sediment (Lake Constance). FEMS Microbiol. Ecol. **73**: 149–158. doi:10.1111/j.1574-6968.1990.tb03935.x

Gregg, M. C., E. A. D'Asaro, J. J. Riley, and E. Kunze. 2018. Mixing efficiency in the ocean. Ann. Rev. Mar. Sci. **10**: 443–473. doi:10.1146/annurev-marine-121916-063643

Gruca-Rokosz, R., and J. A. Tomaszek. (2015). Methane and Carbon Dioxide in the Sediment of a Eutrophic Reservoir: Production Pathways and Diffusion Fluxes at the Sediment–Water Interface. Water Air Soil Pollut. **226**: 16. https://doi.org/10.1007/s11270-014-2268-3

Günthel, M., D. Donis, G. Kirillin, D. Ionescu, H. Grossart, K. W. Tang, M. Bizic, and D. F. Mcginnis. 2019. Contribution of oxic methane production to surface methane emission in lakes and its global importance. Nat. Commun. **10**: 5497. doi:10.1038/s41467-019-13320-0

Harrison, J., B. Deemer, M. K. Birchfield, and M. T. O'Malley. 2017. Reservoir water-level drawdowns accelerate and amplify methane emissions. Environ. Sci. Technol. **51**: 1267–1277. doi:10.1017/CBO9781107415324.004

Henderson, S. M. 2016*a*. Turbulent production in an internal wave bottom boundary layer maintained by a vertically propagating seiche. J. Geophys. Res. Ocean. **121**: 2481–2498.

Henderson, S. M. 2016*b*. Upslope internal-wave Stokes drift, and compensating downslope Eulerian mean currents, observed above a lakebed. J. Phys. Oceanogr. **46**: 1947–1961. doi:10.1175/JPO-D-15-0114.1

Henderson, S. M., and B. R. Deemer. 2012. Vertical propagation of lakewide internal waves. Geophys. Res. Lett. **39**: 1–5. doi:10.1029/2011GL050534

Henderson, S. M., and J. R. Nielson. 2021. Bottom boundary layers, *In* Encyclopedia of inland waters.

Holtappels, M., and A. Lorke. 2011. Estimating turbulent diffusion in a benthic boundary layer. Limnol. Oceanogr. Methods **9**: 29–41. doi:10.4319/lom.2011.9.29

Holtappels, M., M. M. M. Kuypers, M. Schlüter, and V. Brüchert. 2011. Measurement and interpretation of solute concentration gradients in the benthic boundary layer. Limnol. Oceanogr. Methods **9**: 1–13. doi:10.4319/lom.2011.9.1

Horn, D. A., J. Imberger, and G. N. Ivey. 2001. The degeneration of large-scale interfacial gravity waves in lakes. J. Fluid Mech. **434**: 181–207. doi:10.1017/S0022112001003536

Hounshell, A. G., R. P. McClure, M. E. Lofton, and C. C. Carey. 2021. Whole-ecosystem oxygenation experiments reveal substantially greater hypolimnetic methane concentrations in reservoirs during anoxia. Limnol. Oceanogr. Lett. **6**: 33–42. doi:10.1002/lol2.10173

Huttunen, J. T., T. S. Väisänen, S. K. Hellsten, and P. J. Martikainen. 2006. Methane fluxes at the sediment–water interface in some boreal lakes and reservoirs. Boreal Environ. Res. **11**: 27–34.

Ivey, G. N., and J. Imberger. 1991. On the nature of turbulence in a stratified fluid. Part I: The energetics of mixing. J. Phys. Oceanogr. **21**: 650–658.

Jassby, A., and T. Powell. 1975. Vertical patterns of eddy diffusion during stratification in Castle Lake. California. Limnol. Oceanogr. **20**: 530–543. doi:10.4319/lo.1975.20.4.0530

Kankaala, P., J. Huotari, E. Peltomaa, T. Saloranta, and A. Ojala. 2006*a*. Methanotrophic activity in relation to methane efflux and total heterotrophic bacterial production in a stratified, humic, boreal lake. Limnol. Oceanogr. **51**: 1195–1204. doi:10.4319/lo.2006.51.2.1195

Kankaala, P., S. Taipale, J. Grey, E. Sonninen, L. Arvola, and R. I. Jones. 2006*b*. Experimental δ¹³C evidence for a contribution of methane to pelagic food webs in lakes. Limnol. Oceanogr. **51**: 2821–2827. doi:10.4319/lo.2006.51.6.2821

Kankaala, P., S. Taipale, H. Nykänen, and R. I. Jones. 2007. Oxidation, efflux, and isotopic fractionation of methane during autumnal turnover in a polyhumic, boreal lake. J. Geophys. Res. **112**: G02003. doi:10.1029/2006JG000336

Kelly, C. A., and D. P. Chynoweth. (1980). Comparison of In Situ and In Vitro Rates of Methane Release in Freshwater Sediments. Appl. Environ. Microbiol. **40**: 287–293. https://doi.org/10.1128/aem.40.2.287-293.1980

Knoery, J., D. Cossa, B. Thomas, G. Gregory, and S. Rigaud. 2019. Susane, a device for sampling chemical gradients in the benthic water column. Limnol. Oceanogr. Methods **17**: 331–342. doi:10.1002/lom3.10317

Kuivila, K. M., J. W. Murray, A. H. Devol, M. E. Lidstrom, and C. E. Reimers. 1988. Methane cycling in the sediments of Lake Washington. Limnol. Oceanogr. **33**: 571–581. doi:10.4319/lo.1988.33.4.0571

Lemaire, B. J., C. Noss, and A. Lorke. 2017. Toward relaxed eddy accumulation measurements of sediment–water exchange in aquatic ecosystems. Geophys. Res. Lett. **44**: 8901–8909. doi:10.1002/2017GL074625

Li, L., A. Fuchs, S. H. Ortega, B. Xue, and P. Casper. 2021. Spatial methane pattern in a deep freshwater lake: Relation to water depth and topography. Sci. Total Environ. **764**: 142829. doi:10.1016/j.scitotenv.2020.142829

Liikanen, A., H. Tanskanen, T. Murtoniemi, and P. J. Martikainen. 2002. A laboratory microcosm for simultaneous gas and nutrient flux measurements in sediments. Boreal Environ. Res. **7**: 151–160.

Liikanen, A., J. T. Huttunen, T. Murtoneimi, H. Tanskanen, T. Väisänen, J. Silvola, J. Alm, and P. J. Martikainen. 2003. Spatial and seasonal variation in greenhouse gas and nutrient dynamics and their interactions in the sediments of a boreal eutrophic lake. Biogeochemistry **65**: 83–103. doi:10.1023/A:1026070209387

Lorke, A., B. Müller, M. Maerki, and A. Wüest. 2003. Breathing sediments: The control of diffusive transport across the sediment–water interface by periodic boundary-layer turbulence. Limnol. Oceanogr. **48**: 2077–2085. doi:10.4319/lo.2003.48.6.2077

Lorke, A., and S. MacIntyre. 2009. The benthic boundary layer (in rivers, lakes, and reservoirs), p. 505–514. *In* G. E. Likens [ed.], Encyclopedia of inland waters. Elservier.

Lorrai, C., D. F. McGinnis, P. Berg, A. Brand, and A. Wüest. 2010. Application of oxygen eddy correlation in aquatic

systems. J. Atmos. Oceanic Tech. **27**: 1533–1546. doi:10.1175/2010JTECHO723.1

Martinez-Cruz, K., A. Sepulveda-Jauregui, P. Casper, K. W. Anthony, K. A. Smemo, and F. Thalasso. 2018. Ubiquitous and significant anaerobic oxidation of methane in freshwater lake sediments. Water Res. **144**: 332–340. doi:10.1016/j.watres.2018.07.053

Matthews, D. A., S. W., Effler, and C. M. Matthews. (2005). Long-term trends in methane flux from the sediments of Onondaga Lake, NY: Sediment diagenesis and impacts on dissolved oxygen resources. Archiv Für Hydrobiologie, **163**: 435–462. https://doi.org/10.1127/0003-9136/2005/0163-0435

Mayr, M. J., M. Zimmermann, J. Dey, A. Brand, B. Wehrli, and H. Bürgmann. 2020*a*. Growth and rapid succession of methanotrophs effectively limit methane release during lake overturn. Commun. Biol. **3**: 108. doi:10.1101/707836

Mayr, M. J., M. Zimmermann, J. Dey, and B. Wehrli. 2020*b*. Lake mixing regime selects methane-oxidation kinetics of the methanotroph assemblage. Biogeosciences **17**: 4247–4259. doi:10.5194/bg-17-4247-2020

Maerki, M., B. Müller, C. Dinkel, and B. Wehrli. (2009). Mineralization pathways in lake sediments with different oxygen and organic carbon supply. Limnol. Oceanogr. **54**: 428–438. https://doi.org/10.4319/lo.2009.54.2.0428

McGillis, W. R., C. Langdon, B. Loose, K. K. Yates, and J. Corredor. 2011. Productivity of a coral reef using boundary layer and enclosure methods. Geophys. Res. Lett. **38**: 1–5. doi:10.1029/2010GL046179

Miles, J. W. 1961. On the stability of heterogeneous shear flows. J. Fluid Mech. **10**: 496–508. doi:10.1017/S0022112063000707

Monin, A. S., and A. M. Yaglom. 1975. Statistical fluid mechanics: Mechanics of turbulence. Dover.

Monismith, S. G., J. R. Koseff, and B. L. White. 2018. Mixing efficiency in the presence of stratification: When is it constant? Geophys. Res. Lett. **45**: 5627–5634. doi:10.1029/2018GL077229

Murniati, E., S. Geissler, and A. Lorke. 2015. Short-term and seasonal variability of oxygen fluxes at the sediment–water interface in a riverine lake. Aquat. Sci. **77**: 183–196. doi:10.1007/s00027-014-0362-7

Nielson, J. R., and S. M. Henderson. 2022. Bottom boundary layer mixing processes across internal seiche cycles: Dominance of downslope flows. Limnol. Oceanogr. **67**: 1111–1125. doi:10.1002/lno.12060

Nielson, J. R., and S. M. Henderson. n.d. Periodic boundary layer separation and lateral intrusions observed above a sloping lakebed. Limnol. Oceanogr. In Review.

Norði, K. Á., B. Thamdrup, and C. J. Schubert. 2013. Anaerobic oxidation of methane in an iron-rich Danish freshwater lake sediment. Limnol. Oceanogr. **58**: 546–554. doi:10.4319/lo.2013.58.2.0546

Nürnberg, G. K. 2022. Quantification of anoxia and hypoxia in water bodies, pp. 1–9. *In* P. Maurice (Ed.), Encyclopedia of Water. Wiley. doi:10.1002/9781119300762.wsts0081

Osborn, T. R. 1980. Estimates of the local rate of vertical diffusion from dissipation measurements. J. Phys. Oceanogr. **10**: 83–89 doi:10.1175/1520-0485(1980)010<0083:eotlro>2.0.co;2.

Peeters, F., and H. Hofmann. 2021. Oxic methanogenesis is only a minor source of lake-wide diffusive CH4 emissions from lakes. Nat. Commun. **12**: 1–5. doi:10.1038/s41467-021-21215-2

Perkins, K. R., G. Rollwagen-Bollens, S. M. Bollens, and J. A. Harrison. 2019. Variability in the vertical distribution of chlorophyll in a spill-managed temperate reservoir. Lake Reserv. Manag. **35**: 119–126. doi:10.1080/10402381.2019.1566935

Reed, D. C., B. R. Deemer, S. van Grinsven, and J. A. Harrison. 2017. Are elusive anaerobic pathways key methane sinks in eutrophic lakes and reservoirs? Biogeochemistry **134**: 29–39. doi:10.1007/s10533-017-0356-3

Reidenbach, M. A., S. G. Monismith, J. R. Koseff, G. Yahel, and A. Genin. 2006. Boundary layer turbulence and flow structure over a fringing coral reef. Limnol. Oceanogr. **51**: 1956–1968. doi:10.4319/lo.2006.51.5.1956

Reis, P. C. J., S. D. Thottathil, and Y. T. Prairie. 2022. The role of methanotrophy in the microbial carbon metabolism of temperate lakes. Nat. Commun. **13**: 43. doi:10.1038/s41467-021-27718-2

Rodriguez, M., T. Gonsiorczyk, and P. Casper. 2018. Methane production increases with warming and carbon additions to incubated sediments from a semiarid reservoir. Inland Waters **8**: 109–121. doi:10.1080/20442041.2018.1429986

Roland, F. A. E., F. Darchambeau, C. Morana, S. Bouillon, and A. V. Borges. 2017. Emission and oxidation of methane in a meromictic, eutrophic and temperate lake (Dendre, Belgium). Chemosphere **168**: 756–764. doi:10.1016/j.chemosphere.2016.10.138

Rosentreter, J. A., and others. 2021. Half of global methane emissions come from highly variable aquatic ecosystem sources. Nat. Geosci. **14**: 225–230. doi:10.1038/s41561-021-00715-2

Rudd, J. W. M., and R. D. Hamilton. (1978). Methane cycling in a eutrophic shield lake and its effects on whole lake metabolism 1. Limnol. Oceanogr. **23**: 337–348. https://doi.org/10.4319/lo.1978.23.2.0337

Saarela, T., A. J. Rissanen, A. Ojala, J. Pumpanen, S. L. Aalto, M. Tiirola, T. Vesala, and H. Jäntti. 2020. CH4 oxidation in a boreal lake during the development of hypolimnetic hypoxia. Aquat. Sci. **82**: 1–12. doi:10.1007/s00027-019-0690-8

Sauter, E. J., M. Schlüter, J. Wegner, and E. Labahn. 2005. A routine device for high resolution bottom water sampling. J. Sea Res. **54**: 204–210. doi:10.1016/j.seares.2005.04.005

Schwefel, R., M. Hondzo, A. Wüest, and D. Bouffard. 2017. Scaling oxygen microprofiles at the sediment interface of deep stratified waters. Geophys. Res. Lett. **44**: 1340–1349. doi:10.1002/2016GL072079

Schwefel, R., T. Steinsberger, D. Bouffard, L. D. Bryant, B. Müller, and A. Wüest. 2018. Using small-scale measurements to estimate hypolimnetic oxygen depletion in a deep lake. Limnol. Oceanogr. **63**: S54–S67. doi:10.1002/lno.10723

Sharples, J., C. M. Moore, T. P. Rippeth, P. M. Holligan, D. J. Hydes, N. R. Fisher, and J. H. Simpson. 2001. Phytoplankton distribution and survival in the thermocline. Limnol. Oceanogr. **46**: 486–496. doi:10.4319/lo.2001.46.3.0486

Sharples, J., and others. 2007. Spring-neap modulation of internal tide mixing and vertical nitrate fluxes at a shelf edge in summer. Limnol. Oceanogr. **52**: 1735–1747. doi:10.4319/lo.2007.52.5.1735

Smyth, W. D., J. D. Nash, and J. N. Moum. 2005. Differential diffusion in breaking Kelvin–Helmholtz billows. J. Phys. Oceanogr. **35**: 1004–1022. doi:10.1175/JPO2739.1

Steinsberger, T., M. Schmid, A. Wüest, R. Schwefel, B. Wehrli, and B. Müller. 2017. Organic carbon mass accumulation rate regulates the flux of reduced substances from the sediments of deep lakes. Biogeosciences **14**: 3275–3285. doi:10.5194/bg-14-3275-2017

Stillinger, D. C., K. N. Helland, and C. W. Van Atta. 1983. Experiments on the transition of homogeneous turbulence to internal waves in a stratified fluid. J. Fluid Mech. **131**: 91–122. doi:10.2514/6.1983-1704, -1

Strayer, R. F., and J. M. Tiedje. 1978. In situ methane production in a small, hypereutrophic, hard-water lake: Loss of methane from sediments by vertical diffusion and ebullition. Limnol. Oceanogr. **23**: 1201–1206. doi:10.4319/lo.1978.23.6.1201

Takeshita, Y., W. McGillis, E. M. Briggs, A. L. Carter, E. M. Donham, T. R. Martz, N. N. Price, and J. E. Smith. 2016. Assessment of net community production and calcification of a coral reef using a boundary layer approach. J. Geophys. Res. Oceans **5655–5671**: 5655–5671. doi:10.1002/2016JC011886

Thorpe, S. A. 2007. An introduction to ocean turbulence. Cambridge Univ. Press.

Turk, D., and others. 2015. Community metabolism in shallow coral reef and seagrass ecosystems, lower Florida keys. Mar. Ecol. Prog. Ser. **538**: 35–52. doi:10.3354/meps11385

Venayagamoorthy, S. K., and D. D. Stretch. 2010. On the turbulent Prandtl number in homogeneous stably stratified turbulence. J. Fluid Mech. **644**: 359–369. doi:10.1017/S002211200999293X

Wanninkhof, R. H. 1992. Relationship between wind speed and gas exchange. J. Geophys. Res. **97**: 7373–7382. doi:10.1029/92JC00188

West, W. E., J. J. Coloso, and S. E. Jones. 2012. Effects of algal and terrestrial carbon on methane production rates and methanogen community structure in a temperate lake sediment. Freshw. Biol. **57**: 949–955. doi:10.1111/j.1365-2427.2012.02755.x

Wiles, P. J., T. P. Rippeth, J. H. Simpson, and P. J. Hendricks. 2006. A novel technique for measuring the rate of turbulent dissipation in the marine environment. Geophys. Res. Lett. **33**: 1–5. doi:10.1029/2006GL027050

Williams, C., J. Sharples, C. Mahaffey, and T. Rippeth. 2013. Wind-driven nutrient pulses to the subsurface chlorophyll maximum in seasonally stratified shelf seas. Geophys. Res. Lett. **40**: 5467–5472. doi:10.1002/2013GL058171

Wüest, A., and A. Lorke. 2003. Small-scale hydrodynamics in lakes. Annu. Rev. Fluid Mech. **35**: 373–412. doi:10.1146/annurev.fluid.35.101101.161220

Zhang, Y., B. Sun, W. Ju, and others. 2021. Eddy correlation measurements of benthic oxygen fluxes in a stratified and operated reservoir. J. Hydrol. **595**: 126007. doi:10.1016/j.jhydrol.2021.126007

## Conflict of Interest
None declared.